

Award Number: W81XWH-05-1-0570

TITLE: Integration of Diagnostic and Interventional MRI for the Study of Persistent Prostate Cancer after External Beam Radiotherapy

PRINCIPAL INVESTIGATOR: Cynthia Ménard, M.D.

CONTRACTING ORGANIZATION: University Health Network
Toronto, Canada, M5G 1Z5

REPORT DATE: October 2009

TYPE OF REPORT: Final

PREPARED FOR: U.S. Army Medical Research and Materiel Command
Fort Detrick, Maryland 21702-5012

DISTRIBUTION STATEMENT: Approved for Public Release;
Distribution Unlimited

The views, opinions and/or findings contained in this report are those of the author(s) and should not be construed as an official Department of the Army position, policy or decision unless so designated by other documentation.

REPORT DOCUMENTATION PAGE

Form Approved
OMB No. 0704-0188

Public reporting burden for this collection of information is estimated to average 1 hour per response, including the time for reviewing instructions, searching existing data sources, gathering and maintaining the data needed, and completing and reviewing this collection of information. Send comments regarding this burden estimate or any other aspect of this collection of information, including suggestions for reducing this burden to Department of Defense, Washington Headquarters Services, Directorate for Information Operations and Reports (0704-0188), 1215 Jefferson Davis Highway, Suite 1204, Arlington, VA 22202-4302. Respondents should be aware that notwithstanding any other provision of law, no person shall be subject to any penalty for failing to comply with a collection of information if it does not display a currently valid OMB control number. **PLEASE DO NOT RETURN YOUR FORM TO THE ABOVE ADDRESS.**

1. REPORT DATE 1 Oct 2009		2. REPORT TYPE Final		3. DATES COVERED 15 SEP 2005 - 14 SEP 2009	
4. TITLE AND SUBTITLE Integration of Diagnostic and Interventional MRI for the Study of Persistent Prostate Cancer after External Beam Radiotherapy				5a. CONTRACT NUMBER	
				5b. GRANT NUMBER W81XWH-05-1-0570	
				5c. PROGRAM ELEMENT NUMBER	
6. AUTHOR(S) Cynthia Ménard, M.D. E-Mail: cynthia.menard@rmp.uhn.on.ca				5d. PROJECT NUMBER	
				5e. TASK NUMBER	
				5f. WORK UNIT NUMBER	
7. PERFORMING ORGANIZATION NAME(S) AND ADDRESS(ES) University Health Network Toronto, Canada, M5G 1Z5				8. PERFORMING ORGANIZATION REPORT NUMBER	
9. SPONSORING / MONITORING AGENCY NAME(S) AND ADDRESS(ES) U.S. Army Medical Research and Materiel Command Fort Detrick, Maryland 21702-5012				10. SPONSOR/MONITOR'S ACRONYM(S)	
				11. SPONSOR/MONITOR'S REPORT NUMBER(S)	
12. DISTRIBUTION / AVAILABILITY STATEMENT Approved for Public Release; Distribution Unlimited					
13. SUPPLEMENTARY NOTES					
14. ABSTRACT This study involved the technical development and clinical testing of a novel technique for magnetic resonance imaging (MRI) guided prostate biopsy in a 1.5T horizontal bore scanner using a dedicated interventional table. We primarily hypothesize that the integration of diagnostic and interventional MRI enables needle biopsy targeting to foci of tumor recurrence after radiotherapy, and will enable a determination of the diagnostic accuracy of MRI in mapping sub-sites of tumor recurrence after radiotherapy.					
15. SUBJECT TERMS Prostate cancer, magnetic resonance imaging, image-guidance					
16. SECURITY CLASSIFICATION OF:			17. LIMITATION OF ABSTRACT	18. NUMBER OF PAGES	19a. NAME OF RESPONSIBLE PERSON USAMRMC
a. REPORT U	b. ABSTRACT U	c. THIS PAGE U			19b. TELEPHONE NUMBER (include area code)
			UU	63	

Table of Contents

	<u>Page</u>
Introduction.....	1
Body.....	1
Key Research Accomplishments.....	10
Reportable Outcomes.....	10
Conclusion.....	11
References.....	11
Appendices.....	12

INTRODUCTION:

This study involves the technical development and clinical testing of a novel technique for magnetic resonance imaging (MRI) guided prostate biopsy in a 1.5T horizontal bore scanner using a dedicated interventional table. We primarily hypothesized that the integration of diagnostic and interventional MRI enables needle biopsy targeting to foci of tumor recurrence after radiotherapy, and will enable a determination of the diagnostic accuracy of MRI in mapping sub-sites of tumor recurrence after radiotherapy. In this final report, we provide strong evidence supporting our primary study hypothesis.

The clinical trial was designed to enroll patients with suspicion of locally recurrent prostate cancer after external beam radiotherapy in a pilot, three-stage trial design. The first stage included technical development and optimization of the imaging technique. The second stage included technical development and optimization of the biopsy technique, followed by a clinical evaluation stage. Stages 1 and 2 have completed accrual, where 16 patients were enrolled in stage 1, and 4 patients were enrolled in stage 2. Stage 3 continues to accrue, and to date has enrolled 14 patients of a planned target accrual of 30 patients. A companion pilot study investigating profiles of hypoxia has completed accrual with 13 patients and is now closed. The clinical evaluation stage 3 of the trial is expected to close to accrual within the next 12 months.

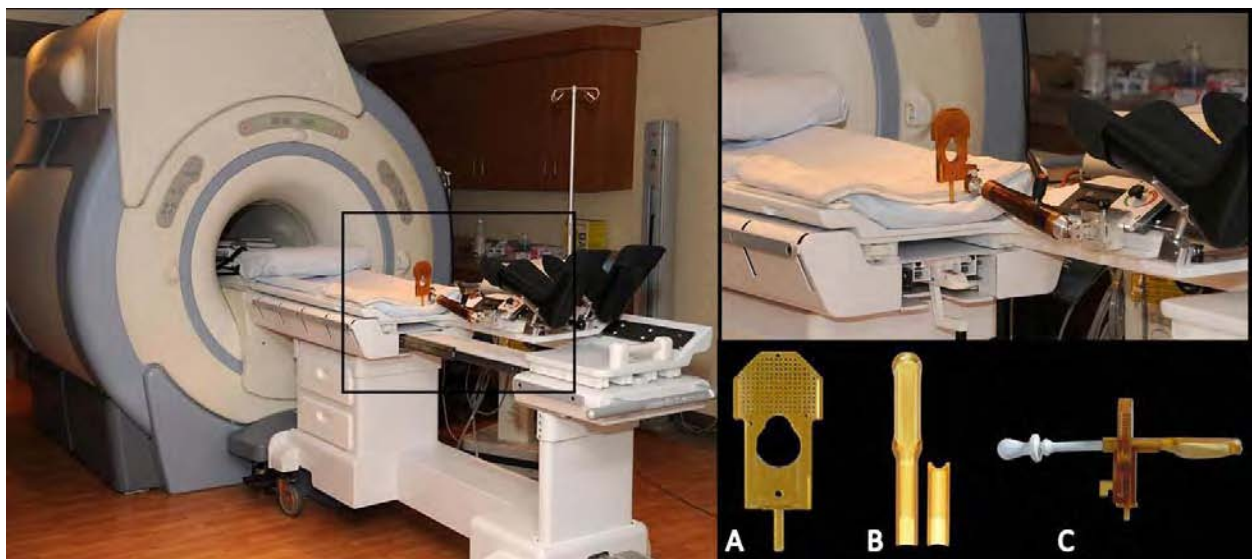
BODY:

USAMRCMC approval for the conduct of the clinical trial was obtained on October 13, 2006, therefore the statement of work was delayed by one year for regulatory approval. Here, we report final and most updated results for each task of the project.

Aim 1: To test the hypothesis that stereotactic MRI-guided prostate needle biopsies can be performed with improved anatomic targeting accuracy and tolerability when patients are positioned supine in a conventional MR scanner.

Task 1a. To design a custom interventional MRI table and hardware system that provides immobilization and perineal access in the supine position.

The table and hardware system has been designed in collaboration with industry (Sentinelle Medical Inc.), and our current system (depicted below) is the third prototype now scheduled for product release in 2010. The navigation system provides access to the perineum in an immobilized supine patient position within a 1.5T GE Signa scanner, and a stereotactic transperineal template assembly which integrates a commercial endorectal imaging coil (C - Medrad Inc.). The pelvis and legs are immobilized using velcro straps.



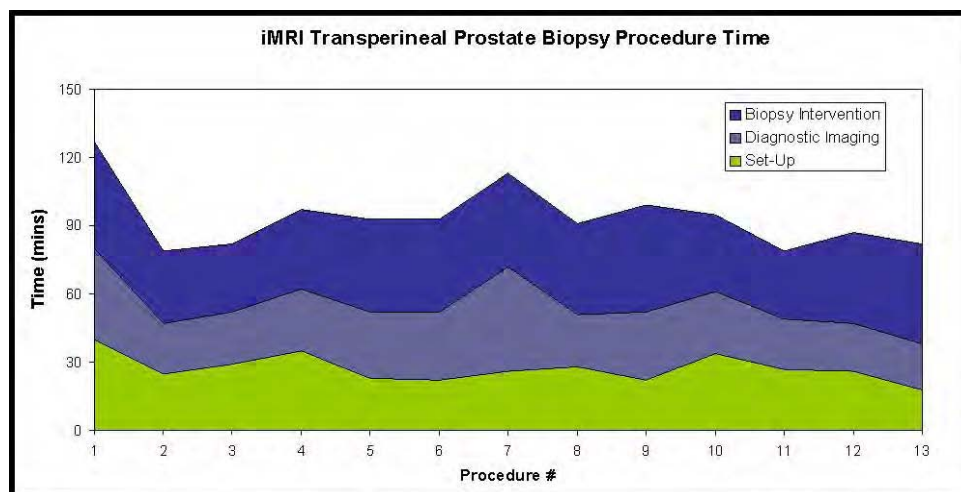
Task 1b. To measure prostate motion while patients are immobilized on the custom table.

Prostate motion was measured by identifying 3D fiducial reference points visible on both the registration T2 images at the beginning of the procedure, and again on the first and last needle verification image. The majority of reference points consisted of implanted gold marker visualized as an area of hypointensity on T2 FSE images. Where gold markers were not present, distinct anatomic points of hyper or hypointensity were used. Prostate motion was determined by averaging displacements of all visible points in a given image pair. Between the T2 images used for guidance and needle verification images after insertion of the first biopsy needles, median vector displacement for the entire cohort was 1.3 mm (SD 1.0, Max 3.2). The largest displacements were observed in the SI dimension, where image resolution was 3mm, and along the trajectory of force applied by needles. Similarly, there was minimal prostate displacement between the registration T2 images and final needle verification image, with a median (SD) vector displacement of 3.1 mm (1.5), within image spatial resolution. This data support the hypothesis that our positioning and sedation protocol minimizes prostate motion, and enables stereotactic needle targeting under the assumption of a static system.

Task 1c. To measure tolerance and feasibility of the integrated diagnostic and interventional procedure.

Patient in the evaluation cohort (stage 3) underwent the integrated diagnostic and biopsy procedure under propofol sedation. As such, pain and tolerability VAS scores were reported to be 0 in all but one patient, who reported a 0.5 score (out of 10 points, 0=no pain/discomfort, 10=worst possible pain/discomfort). Regarding adverse events, one patient experienced a Grade 3 pulmonary embolism within a few days of the biopsy procedure. He was investigated and found to have a hypercoagulable syndrome, and the event was deemed unlikely to be related to the procedure. A second patient experienced a Grade 2 vasovagal hypotensive event 1 hour after the procedure which resolved with conservative measures. No patients experienced an infection or other complications related to the biopsy procedure.

Feasibility metrics included the following: frequency of visible suspicious tumor targets for biopsy, frequency of complete biopsy sampling, and procedure times. Of 14 patients enrolled to date in stage 3 of the trial, one procedure was aborted due to MRI scanner malfunction. All thirteen evaluable patients had regional MRI features suspicious for cancer and specifically targeted for biopsy. Intended biopsy sampling (tumor targets + a minimum of sextant sampling) was successfully achieved in 10 patients. Insufficient diagnostic sampling was observed in the first two patients due to poor core quality, which led to a change manual handling of the MRI compatible biopsy gun. A later patient had insufficient sampling due longer needle length requirements (thick perineal fat), and subsequent procedures utilized longer biopsy guns (175mm instead of 150mm). The number of biopsy cores sampled per patient ranged from 8-13. Mean diagnostic MRI + biopsy procedure time was 76 min (56-93 min). For each needle verification interval, two biopsies were acquired from targets in the right and left lobes of the gland. The mean time for needle insertion, needle verification, and biopsy acquisition for a biopsy interval was 7.5 min (5.8-11.6min). After patient 5, set-up was performed in the MRI scanner suite. Trends in time performance are depicted below through the course of the study.



Task 1d. To confirm the geometric needle targeting accuracy of the supine trans-perineal system in a gel phantom.

A phantom experiment was conducted using Aegis targeting software, and Prostate Phantom (Model 053, CIRS Inc.), as well as Invivo 16 gage automatic biopsy gun. Mean needle targeting accuracy (n=7) was: $x=0.34 \pm 0.31$ mm, and $y=-1.57 \pm 1.09$ mm. A posterior systematic but submillimeter bias can be addressed by re-calibrating the device. This phantom data was reported at the ISMRM Annual meeting in 2007. (1,2) Results indicate high performance of the needle navigation system, and was deemed sufficiently accurate to proceed with clinical testing.

Task 1e. To test the geometric and anatomic needle targeting accuracy of the supine trans-perineal system in patients with suspected local persistence of prostate cancer after external beam radiotherapy.

The navigation system is a fundamental component of image guided prostate cancer targeting. The following figure illustrates the feedback relationships designed to improve prostate cancer targeting accuracy of the navigation system.

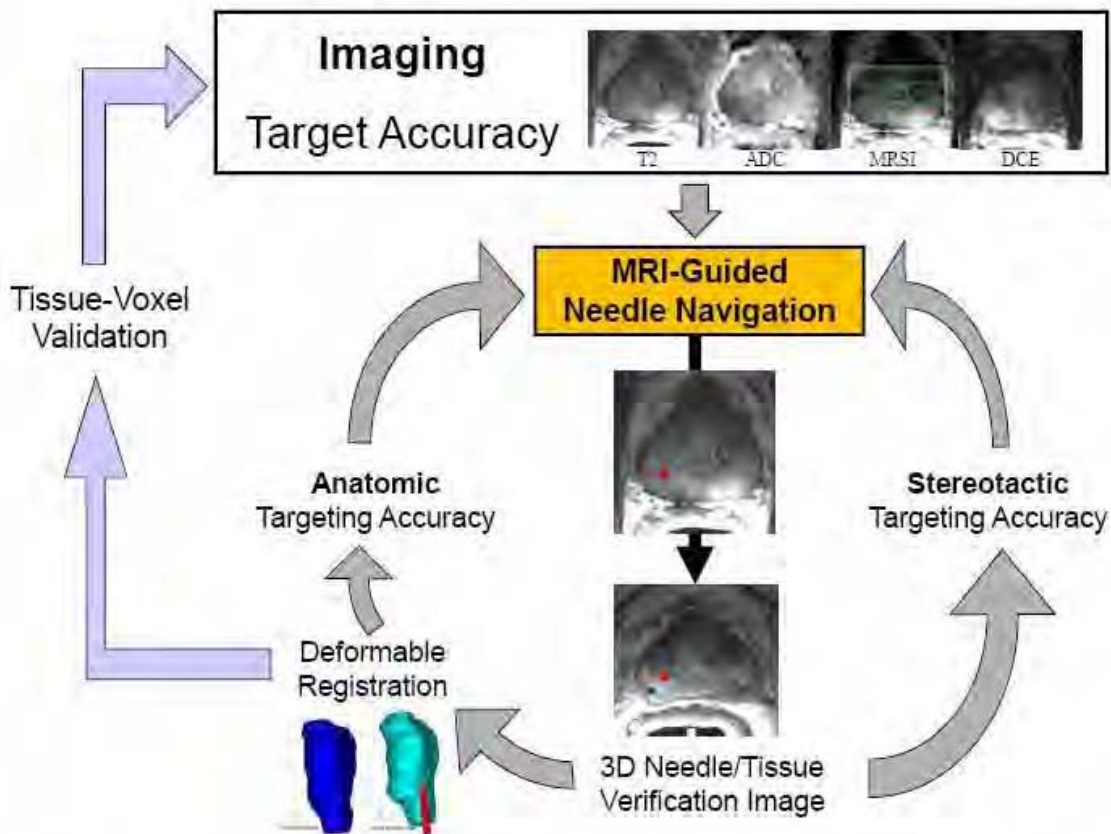
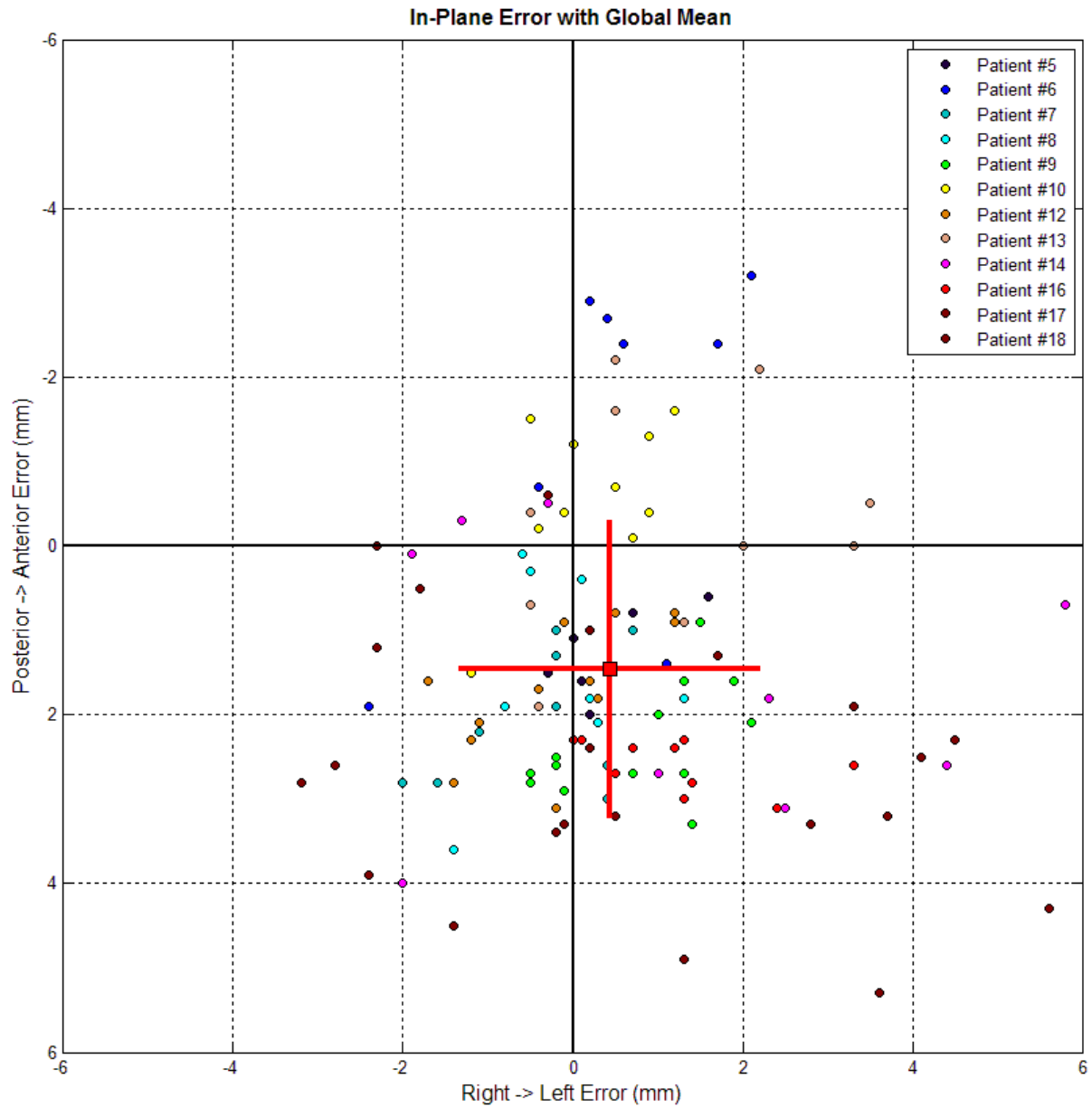
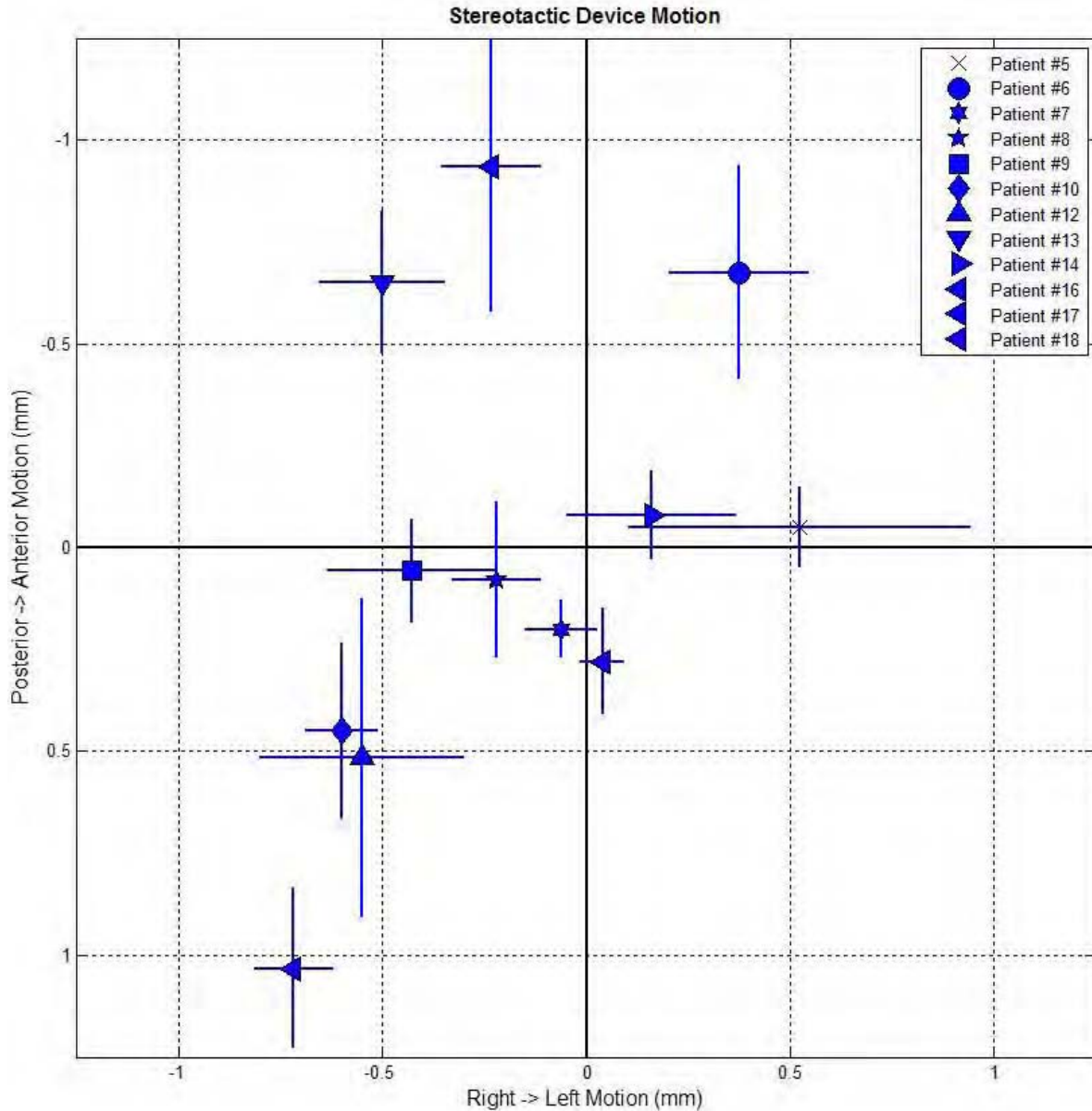


Figure 1 - Illustration of the feedback relationships designed to improve targeting accuracy of the navigation system. General MRI features of prostate cancer (nodular area of hypointensity on T2 weighted images, low apparent diffusion coefficient, elevated choline relative to citrate, and intense and rapid contrast enhancement and washout visualized here in the right peripheral zone) are used to identify suspicious imaging targets for biopsy (red target). 3D needle verification images are used to assess and improve the stereotactic performance of the navigation system by comparing the actual needle location (dark signal void) to that intended (red target) in stereotactic space. These images, in conjunction with deformable image registration, can also provide metrics of anatomic needle targeting accuracy. This data can be used to create needle deformation models that could be incorporated into the navigation system for improved needle targeting. Most importantly, 3D needle/tissue verification images and deformable image registration enable accurate voxel-to-tissue co-localization that will validate and help refine quantitative MRI parameters diagnostic of cancer burden and biological virulence, thereby improving imaging target accuracy.

The inplane stereotactic targeting accuracy was calculated by finding the distance between the actual needle and the intended target location in MRI coordinates. The actual needle location was recorded as the center of the signal void visible in the needle verification images. For a total of 121 needle targets in 12 patients, the mean (SD) in plane targeting accuracy in millimeter was $x=0.44$ (1.77), $y=1.46$ (1.77), and vector 2.57 (1.41). The inplane error was distributed randomly in the right to left direction but a small posterior systematic bias of the inplane errors of approximately 1 mm was observed. The following figure depicts all stereotactic needle target errors as well as the mean (SD) for the entire cohort, with each needle considered an independent variable. As needle targets within a given patient are unlikely to be independent variables, we also computed the mean (SD) for each patient. Across patients, the mean vector targeting error was 2.5 mm (range 1.2 – 4.7 mm).



In keeping with prostate motion data, hardware motion was minimal throughout the biopsy procedures, with a mean hardware motion of 0.64mm (SD 0.39mm), lending credence to the stereotactic guidance assumptions of a stable system.



Anatomic targeting accuracy will be determined by measuring the vector discrepancy between the intended anatomic target for biopsy, and sampled region as visualized on needle verification images. Analysis is ongoing, using 3D maps and FEM deformable registration techniques based on the prostate surface boundary manually delineated on MRI.

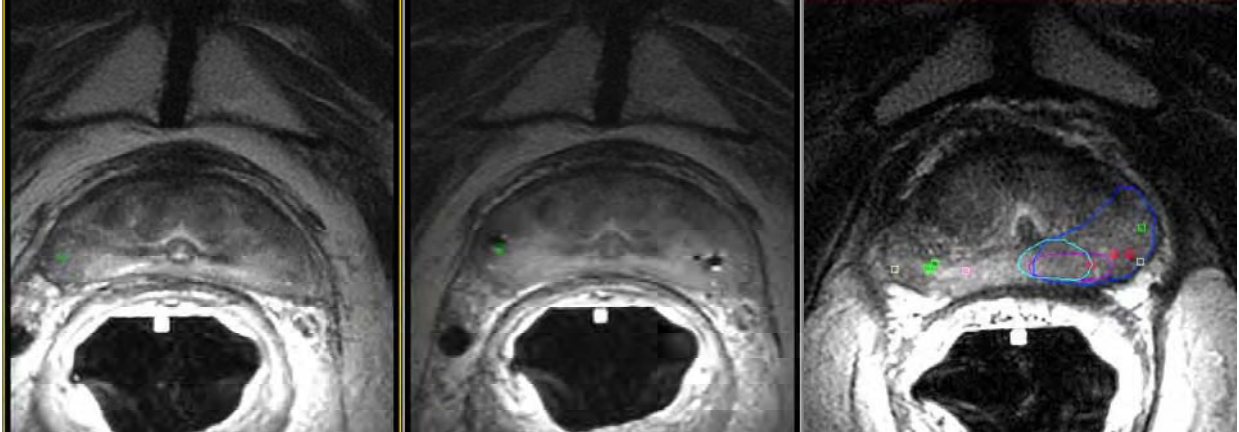
It is our impression based on this data that the majority of targeting inaccuracies occur due to needle deflection at the prostate boundary, which is more pronounced for targets located at the margins of the prostate gland. Ongoing analysis will attempt to model and predict for needle deflection in order to improve overall targeting accuracy of the system.

Gland deformation is minimal with a transperineal approach, but needle insertion does slightly translate the gland superiorly, as previously reported by others. Further work will continue to refine accurate and responsive registration of the stereotactic system, model and account for needle deflection and prostate translation for improved targeting performance.

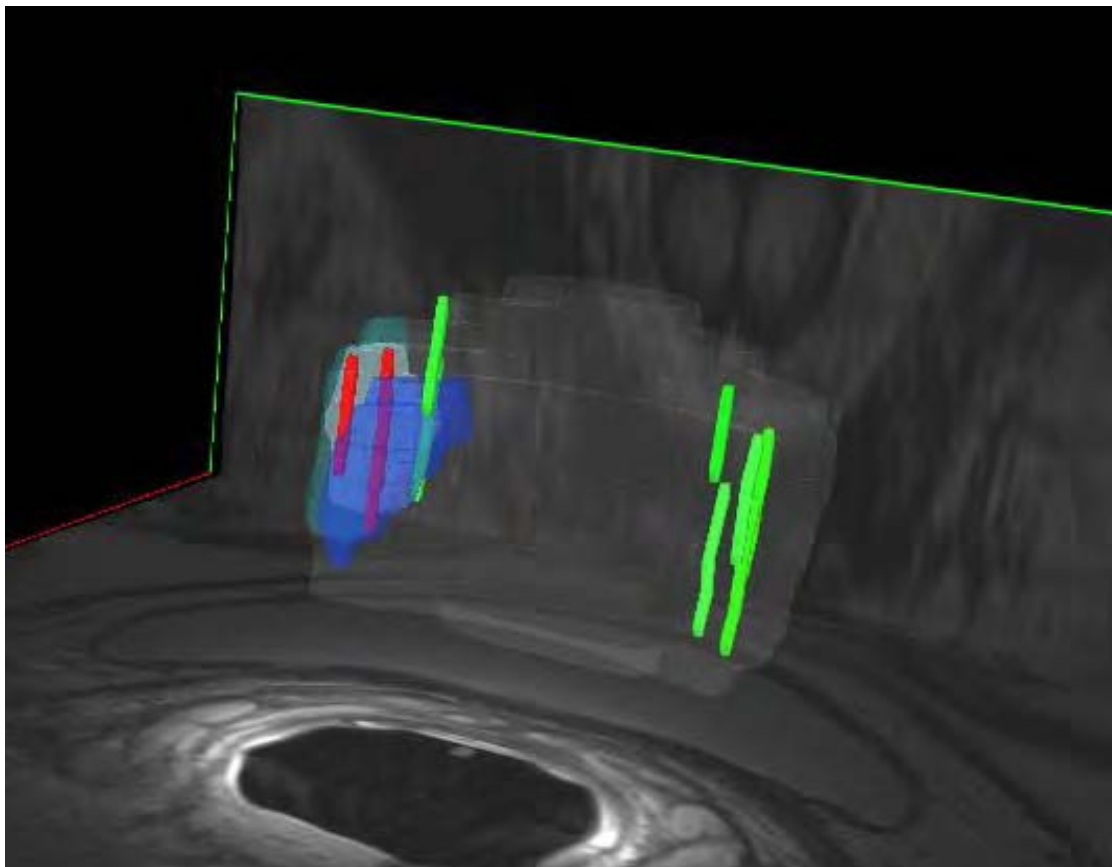
Aim 2: To test the hypothesis that stereotactic MRI-guided needle biopsies will enable the spatial delineation of local prostate cancer persistence after radiotherapy.

Task 2a. To create 3D maps of malignant biopsy sites in reference to MRI prostate anatomy.

3D maps of malignant biopsy sites in reference to MRI prostate anatomy have been successfully generated in all patients. A case example is depicted in the following figure. In b) navigation software (Aegis, Sentinelle Medical Inc.) displays needle target (green) onto diagnostic T2 images. In c) needle verification images document the actual location of 3 biopsy needles (signal voids R and L) in reference to intended target (green). In d), a map of benign (green), malignant-dense (red), malignant-microfocus (pink), and indeterminate (white) biopsy cores are depicted in reference to imaging features suspicious for tumor on DCE (light blue), ADC (purple), and T2 (royal blue). In this case, the boundary of the T2-visible tumor was later revised posteriorly based on a benign biopsy core in this region.



This tumor map can be rendered in 3D, as depicted below for a different patient with a tumor visualized and pathologically confirmed in the right lateral lobe of the gland.



Task 2b. To correlate biopsy tissue histology with spatially corresponding diagnostic MRI data.

The median age at study accrual was 72 years (63-84). All received RT (+/- hormones) for intermediate (n=13) or low-risk (n=2) prostate cancer at initial diagnosis. The median EBRT dose was 75.6Gy (60-79.8 Gy). Only 2 patients received neoadjuvant hormone therapy for a period of 5 months. The median PSA at the time of biopsy was 3.8 ng/ml (2.9-7.9). The median time from RT to biopsy was 5.8 years (1.7-11.4).

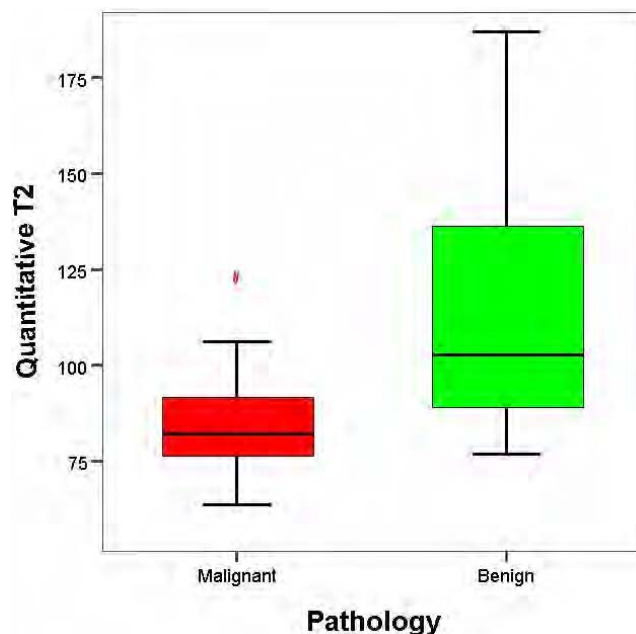
Of 13 evaluable patients evaluable to date, 10 patients were found to have recurrent cancer on their MRI-guided biopsy. The majority of patients had Gleason score 7 recurrence disease (n=7, Gleason score range 6-9). The site of recurrence corresponded to suspicious imaging findings in all but 2 patients. In one patient the malignant biopsy did not spatially correspond with a suspicious imaging focus. In the second patient, disease was diffusely distributed throughout the gland and no focus of disease could be delineated. In all patients with focal recurrences, only 1 focus of disease was present. Extracapsular extension of disease was identified in 2 patients.

Ongoing analysis will have 2 separate expert observers delineate regions that they consider suspicious for tumor-burden based on multiparametric MRI. Overall accuracy (sensitivity/specificity) of the experts will be determined based on co-registered biopsy data. (Collaboration M. Haider)

Task 2c. To define a profile of MRI measurements that accurately delineates sites of tumor persistence within the prostate gland after external beam radiotherapy.

Imaging of actual needle core locations enabled the identification of corresponding imaging voxels on diagnostic images. Once the corresponding 3D location was identified on T2, a 1x1 mm area (corresponding to biopsy size and representing 1.2 voxels) was delineated on sequential slices corresponding to the reported length of biopsy core. The average and standard deviation of voxel values contained within each volume was calculated. Mean T2 was then derived for each biopsy location. While up to 3 slices (representing the entire biopsy length) were included to derive quantitative metrics for benign cores, only slices corresponding to tumor (as estimated from distance between inked end to tumor) were used to derive quantitative metrics for the malignant cores. Quantitative metrics derived from biopsies containing microfoci (defined as a single focus less than or equal to a 40 x microscopic field) (Allan RW, Journal of Urology, 2003;) or less than 5% of involved core were excluded from analysis.

Six patients with quantitative T2 images acquired at the time of biopsy have been analyzed to date, for a total of 45 sampled regions. There was a statistically significant difference in mean T2 between benign (85ms) and malignant (114ms) cores (p=0.02), although substantial overlap remains in the range of T2 values, and no threshold value can accurately distinguish benign and malignant disease (following figure).



A similar quantitative analysis is ongoing to investigate the potential for other quantitative metrics (K_{trans}, ADC, Choline+Creatine/Citrate) to distinguish benign and malignant tissue voxels. Multivariate analysis will then proceed to determine which combination of quantitative threshold achieves the highest diagnostic accuracy in delineating tumor.

Aim 3: To test the hypothesis that integrated diagnostic and interventional MRI will enable the biological characterization of prostate cancer persistence within the prostate gland after radiotherapy.

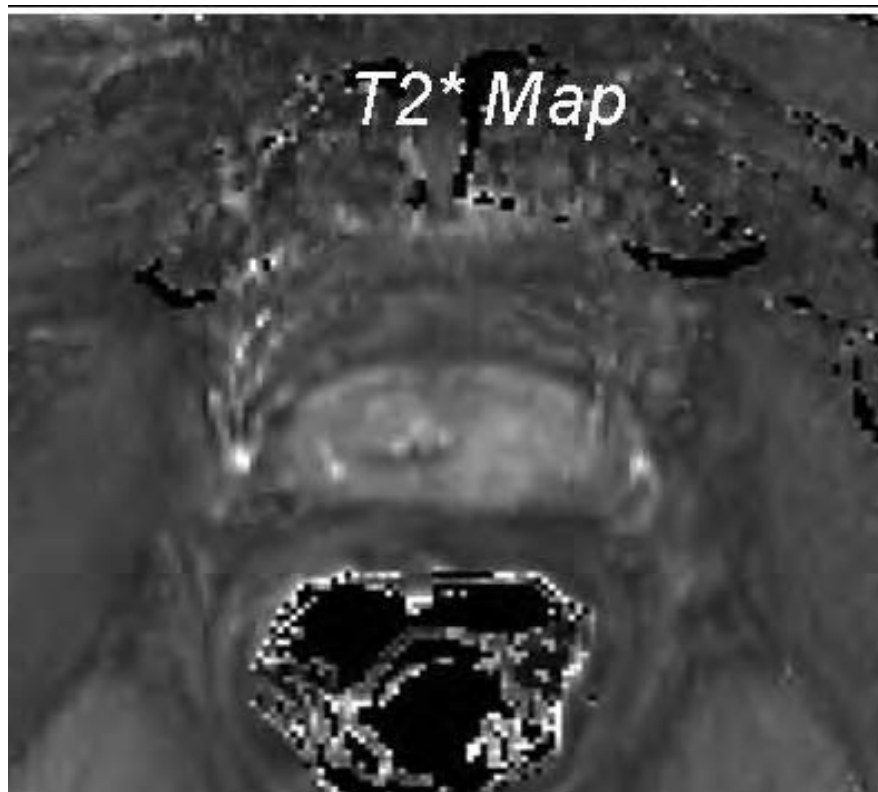
Task 3a. To obtain stereotactic measures of tumor hypoxia.

Thirteen patients received an infusion of Pimonidazole ($0.5\text{mg}/\text{m}^2$) over 20 minutes approximately 18 hours prior to the biopsy to serve as an immunohistochemical biomarker of tumor hypoxia. An example of a needle core acquired under stereotactic MRI guidance and stained with an antibody to Pimonidazole is depicted below. Staining and analysis of the complete cohort is ongoing (collaboration Dr. R. Bristow).



Task 3b. To correlate measures of tumor hypoxia with spatially corresponding MRI data.

T2*/Blood Oxygen Level Dependent (BOLD) MRI image sequences are thought to provide estimates of tissue oxygenation depending on variable magnetic properties of oxy and deoxyhemoglobin. All 13 patients in the companion cohort had quantitative T2* images acquired immediately prior to the biopsy (image example below). One Pimonidazole staining and quantification is complete, voxel/pathological correlation will proceed using the methodology described in Task 2c.



KEY RESEARCH ACCOMPLISHMENTS:

- Design of a system for integrated diagnostic and interventional MRI using stereotactic transperineal needle navigation.
- Clinical demonstration of feasibility, tolerance, target stability, and targeting accuracy of the procedure.
- Raising the importance and value of 3D verification imaging in imaging/pathological correlative investigations.
- Demonstration that recurrent prostate cancer after radiotherapy can usually be localized to a single focus of disease visible on MRI, which can be targeted for biopsy.
- Preliminary evidence that quantitative T2 may contribute in distinguishing tumor from benign tissue.

REPORTABLE OUTCOMES:

- Un-published abstracts presented at meetings

Suljendic D, Lee J, Chopra S, Kirilova A, Publicover J, Abed J, Haider M, Krieger A, Fichtinger G, Brock K, Ménard C. MRI Guided Needle Navigation in Prostate Cancer Targeting. Focal Therapy and Imaging in Prostate and Kidney Cancer. Amsterdam, Netherlands. June 2009

- Published abstracts

Bootsma GJ, Krieger A, Iordachita II, Piron C, Richmond J, Sela G., Filletti M, Rocca C, Kirilova A, Brock K, Jaffray DA, Haider MA, Ménard C. A System for Prostate Interventional in a 1.5T MRI Scanner in the Supine Position. Proc Intl Soc Mag Reson Med 15, 483, 2007.

Ménard C, Bootsma G, Piron C, Sela G, Richmond J, Gallop D, Filletti M, Rocca C, Kirilova A, Iordachita I, Krieger A, Jaffray D, Haider M. A Supine System for Needle-Based Prostate Interventions in a Cylindrical MRI Scanner. Radiother Oncol 84(2):S4, 2007.

Lee J, Brock K, Beiki-Adarkani A, Jezioranski J, Abed J, Publicover J, Morton G, Pouliot J, Haider M, Menard C. Technique for Accurate GTV definition in MR-guided HDR brachytherapy. *Accepted, plenary paper, American Brachytherapy Society, April 2010.*

- Book Chapters

Ménard C, Crook J. The use of Image-Guidance in Prostate Brachytherapy. In Valicenti R, Dicker AP, Jaffray DA. Image-Guided Therapy of Prostate Cancer. New York, NY: Informa Healthcare; Chapter 15, pp. 167-181, 2008.

- Manuscripts

Foltz W, Haider M, Chung P, Bayley A, Catton C, Ramanan V, Jaffray D, Ménard C. Clinical Prostate T1 Quantification Using a Magnetization-Prepared Spiral Technique. J Magn Res Imag Submitted Dec 2009.

Foltz W, Chopra S, Chung P, Bayley A, Catton C, Jaffray D, Haider M, Ménard C. Clinical Prostate T2 Quantification Using a Magnetization-Prepared Spiral Technique. Magn Res Med Submitted Dec 2009

Ménard C, Haider M, Chung P, et al. Development, feasibility, technical performance, and clinical application for MRI-guided prostate biopsy. In preparation

Ménard C, Haider M, Chung P, et al. Accuracy of MRI-guidance to sites of cancer recurrence after radiotherapy for prostate cancer. In preparation

Chopra S., Foltz W. Haider M., et al. Spatial evaluation of hypoxia and local recurrence after radiotherapy for prostate cancer.
In preparation

Chopra S., Toi A., Haider M., et al. Pathological predictors for site of local recurrence after radiotherapy for prostate cancer.
In preparation

Ménard C, Haider M, Chung P, et al. Biopsy-Voxel validation of multiparametric MRI after radiotherapy for prostate cancer.
In preparation

Lee J, Menard, Brock, et al. Variable gland deformation with endo-rectal coil and needle insertion, and registration strategies.
In preparation.

- Trainees

Supriya Chopra, MSc Candidate, University of Toronto, Faculty of Medicine
EIRR21st CIHR Strategic Training Program in Radiation Medicine Award 2008-2009
PMH-UHN Trainee Award In Prostate Cancer Research – 2008-2009
ACURA grant award 2008
NCIC Salary award 2009

Dennis Suljendic, MSc Graduate, University of Toronto, Faculty of Engineering
NSERC scholarship award 2008-2009

- New grants awarded

Multiparametric MRI based evaluation of hypoxia in men with prostate cancer. Sponsor: Abbott-CARO Uro-Oncologic Radiation Award (ACURA) 2008. Amount: 43,000\$ CDN

MRI Guided and Tumor Targeted HDR Brachytherapy for Recurrent Prostate Cancer Sponsor: National Institute of Health #1R21CA121586-01A2 Amount: 274,000\$ USD total for 2 years

Robotic Positioning for Image-guided Surgery and Radiation Therapy Sponsor: Ontario Research Fund / Canadian Foundation for Innovation Amount: 16,030,160\$ CDN total for 4 years

- Awards

CIHR New Investigator Award.

CONCLUSIONS:

Feasibility of integrating multi-parametric MRI for online guidance of prostate biopsy is demonstrated. The value of 3D imaging to document actual location of biopsy cores in reference to anatomic boundaries cannot be overstated. Online MRI needle guidance systems with accurate and responsive navigation help better define cancer features on MRI and enable tumor-targeted diagnostics and therapeutics. Future work will complete the ongoing analysis, and expand investigations to a broader cohort of patients.

REFERENCES:

1. Bootsma GJ, Krieger A, Iordachita II, Piron C, Richmond J, Sela G., Filletti M, Rocca C, Kirilova A, Brock K, Jaffray DA, Haider MA, Ménard C. A System for Prostate Interventional in a 1.5T MRI Scanner in the Supine Position. Proc Intl Soc Mag Reson Med 15, 483, 2007.
2. Ménard C, Bootsma G, Piron C, Sela G, Richmond J, Gallop D, Filletti M, Rocca C, Kirilova A, Iordachita I, Krieger A, Jaffray D, Haider M. A Supine System for Needle-Based Prostate Interventions in a Cylindrical MRI Scanner. Radiother Oncol 84(2):S4, 2007.

APPENDICES:

A - Published Abstract: Bootsma GJ, Krieger A, Iordachita II, Piron C, Richmond J, Sela G., Filleti M, Rocca C, Kirilova A, Brock K, Jaffray DA, Haider MA, Ménard C. A System for Prostate Interventional in a 1.5T MRI Scanner in the Supine Position. *Proc Intl Soc Mag Reson Med* 15, 483, 2007.

B - Published Abstract: Ménard C, Bootsma G, Piron C, Sela G, Richmond J, Gallop D, Filleti M, Rocca C, Kirilova A, Iordachita I, Krieger A, Jaffray D, Haider M. A Supine System for Needle-Based Prostate Interventions in a Cylindrical MRI Scanner. *Radiother Oncol* 84(2):S4, 2007.

C – Accepted Abstract: Lee J, Brock K, Beiki-Adarkani A, Jezioranski J, Abed J, Publicover J, Morton G, Pouliot J, Haider M, Menard C. Technique for Accurate GTV definition in MR-guided HDR brachytherapy. *Accepted, plenary paper, American Brachytherapy Society, April 2010.*

D – Manuscript: Foltz W, Haider M, Chung P, Bayley A, Catton C, Ramanan V, Jaffray D, Ménard C. Clinical Prostate T1 Quantification Using a Magnetization-Prepared Spiral Technique. *J Magn Res Imag* Submitted Dec 2009.

E – Manuscript: Foltz W, Chopra S, Chung P, Bayley A, Catton C, Jaffray D, Haider M, Ménard C. Clinical Prostate T2 Quantification Using a Magnetization-Prepared Spiral Technique. *Magn Res Med* Submitted Dec 2009

A System for Prostate Intervention in a 1.5 T MRI Scanner in the Supine Position

Bootsma GJ, Krieger A, Iordachita II, Piron C, Richmond J, Sela G, Filletti M, Sie F, Rocca C, Kirilova A, Brock K, Jaffray DA, Haider MA, Ménard C

Introduction: Prostate cancer is the most likely cancer to develop in a Canadian male with a prevalence of 1 in 7.1 cases in 2005 [1]. In the United States 230,000 new cases of prostate cancer have been projected for 2005 [2]. Despite improvements in the delivery and reduction in associated toxicity of external beam radiotherapy, local persistence or recurrence of disease remains prevalent in 25-51% of patients [3,4]. A careful and thorough investigation of the spatial distribution of cancer within the prostate gland is paramount to meaningful progress in effective prospective management and therapy for salvage. Magnetic Resonance Imaging (MRI) provides the ability to deliver excellent soft tissue contrast and resolution of the anatomy. It also provides an opportunity to spatially characterize pathology and biology through dynamic contrast-enhanced (DCE) imaging, MR spectroscopic imaging of tissue metabolites, and diffusion-weighted (DWI) imaging. Previous systems have been developed for prostate interventions in a standard 1.5 T MRI scanner with excellent biopsy-needle targeting accuracy, but have required the patient to be placed in the prone or left lateral decubitus position [3], thereby compromising stability, patient comfort, and safety. A number of recent studies have shown that prostate motion is greatly reduced when patients are placed in the supine position due to greater patient comfort and reduced respiratory motion [4-6]. In this work, the feasibility of creating adequate perineal exposure for prostate interventions in the supine position using dedicated table architecture is investigated.



Figure 1: Picture of the custom imaging table for patient positioning in the supine position docked to GE 1.5 T MRI scanner.



Figure 2: Image showing the accessibility of the perineum and accommodation of stereotactic perineal template and coil.

Materials/Methods: To permit the patient to be positioned supine and allow access to the perineum a dedicated prostate interventional table (Figure 1) was designed in collaboration with Sentinel Medical Inc. (Toronto, Canada). The table is a modification of Sentinel Medical's Vanguard System which is used in breast imaging and intervention. The table has been revised to provide boot supports for hip and knee flexion and immobilization, pelvic immobilization, imaging coil integration, and ample room for perineal exposure and operative space (Figure 2). The table has also been designed to accommodate both the "access to prostate tissue under MRI guidance" (APT-MRI) device [7,8] as well as a stereotactic perineal template and coil system [3]. The interventional table provides ease of mobility between the MRI suite and adjacent rooms. Patients can then be set-up on the table prior to it being docked to the MRI scanner, thus freeing the unit for standard clinical workflow. An REB/HSRBB approved protocol is currently enrolling patients to develop the revised interventional techniques and measure organ motion and patient comfort in the new system. Prostate motion was measured using a 2D FIESTA with fat saturation (TE/TR – 1.9/6.2ms; matrix 320x224, FOV 26 cm, 8mm slice thickness) and temporal resolution 2sec, and analyzed with manual POI tracking using MIPAV software (Medical Image Processing Analysis and Visualization – NIH).

Results: On an initial trial, the patient was placed on the table and imaged for a period of 60 minutes with the endorectal coil in place. There was no report of discomfort from the patient, and perineal exposure was excellent (Figure 2). Respiratory and peristaltic motion observed during the 2D FIESTA sequence

caused negligible movement of the prostate gland. Maximum displacement of the prostate gland was 0.51mm and 1.02mm, associated with a mean displacement of 0.00 +/-0.31mm and 0.00 +/-0.31mm in the AP and SI directions, respectively.

Conclusions: Our new system for prostate intervention provides a means by which MRI data can be used to accurately guide intervention as well as provide feedback to validate new imaging techniques with the patient placed in the supine position minimizing patient discomfort and prostate motion.

References: [1] NCIC: Canadian Cancer Statistics 2005, Toronto, Canada 2005. [2]Jemal A. CA Cancer J Clin, 2005;55(1):10-30. [3] Susil RC. Magn Reson Med 2004;52(3);683-7. [4] Mah D. Int J Radiat Oncol Biol Phys 2002;54(2):568-75. [5] Kitamura K. Int J Radiat Oncol Biol Phys 2002;53(5); 1117-23. [6] Bayley AJ. Radiother Oncol 2004;70(1):37-44. [7] Susil RC. Radiology 2004;228(3):886-94. [8] Krieger A. IEEE Trans Biomed Eng 2005; 52(2):306-13.

A Supine System for Needle-Based Prostate Interventions in a Cylindrical MRI Scanner

C. Menard, G. Bootsma, C. Piron, G. Sela, J. Richmond, D. Gallop, M. Filletti, C. Rocca, A. Kirilova, I. Iaordachita, A. Kriger, D. Jaffay, M. Haider

Introduction: A careful and thorough investigation of the spatial distribution of cancer within the prostate gland is paramount to progress in effective tumour-targeted therapy. MRI provides an opportunity to characterize the distribution of glandular pathology and biology. Previous interventional MRI systems have positioned patients in prone or left lateral decubitus, thereby compromising stability, patient comfort, and safety. In the first aim of this work, we sought to determine the feasibility of creating adequate perineal exposure for prostate interventions in the supine position using dedicated table architecture.

Methods: An interventional table was designed providing leg and pelvic immobilization, imaging coil integration, fixation arms for interventional hardware, operative space with perineal exposure, and ease of transfer between MRI and other interventional suites. Patients were enrolled on the 'run-in' phase of a clinical trial in order to develop the interventional techniques and measure organ motion in the new system. Prostate motion was measured using sagittal 2D FIESTA (temporal resolution 2sec), and analyzed using manual POI tracking.

Results: Six patients with suspicion of local recurrence after EBRT have been enrolled and investigated on the system to date. Exposure was adequate for transperineal intervention in all cases. Respiratory and peristaltic motion observed in one patient during the 2D FIESTA sequence caused negligible movement of the prostate gland, with maximum and mean (SD) displacements of 0.51mm and 0mm (0.31mm) in the AP direction, and 1.02mm and 0mm (0.46mm) in the S1 dimension. Recurrent tumour was visualized on MRI, and confirmed on subsequent TRUS-guided biopsy in 5/6 patients.

Conclusions: The new system for prostate intervention provides an improved means for online MRI guidance of needlebased interventions (biopsy and brachytherapy). In next steps, MRI-guided prostate biopsies will be performed in patients suspected of local recurrence after radiotherapy.

Technique for Accurate GTV Definition in MR-Guided HDR Prostate Brachytherapy

Jenny Lee, M.Math (1), jenny.lee@rmp.uhn.on.ca
Kristy Brock, PhD (1, 2), Kristy.Brock@rmp.uhn.on.ca
Akbar Beiki-Ardakani, M.Sc (1), Akbar.Beiki-Ardakani@rmp.uhn.on.ca
John Jezioranski, M.Math (1), John.Jezioranski@rmp.uhn.on.ca
Jessy Abed, RTT (1), Jessy.Abed@rmp.uhn.on.ca
Julia Publicover, M.Sc(1), Julia.Publicover@rmp.uhn.on.ca
Gerard Morton, MD (2,3), Gerard.Morton@sw.ca
Jean Pouliot, PhD (4), JPouliot@radonc.ucsf.edu
Masoom Haider, MD (1, 2), M.Haider@utoronto.ca
Cynthia Ménard, MD (1, 2), Cynthia.Menard@rmp.uhn.on.ca

1)Princess Margaret Hospital, University Health Network - Radiation Medicine Program and Department of Medical Imaging, Toronto, Ontario, M5G 2M9, Canada

2)University of Toronto, Faculty of Medicine - Departments of Radiation Oncology, Medical Imaging, and Medical Biophysics, Toronto, Ontario.

3) Odette Cancer Centre, Radiation Oncology, Toronto, Ontario, M4N 3M5

4) University of California San Francisco, Department of Radiation Oncology, San Francisco, California, 94143, US

Purpose

Despite a strong rationale and enthusiasm for distinguishing regions of tumor-dense burden within the prostate gland for specific dose delivery, methods and tools for clinical investigation have not yet matured. A technique is presented for integrating pathologically referenced multiparametric MRI using deformable registration for HDR brachytherapy planning.

Methods

Four patients enrolled on a prospective trial of tumor-targeted MRI-guided HDR salvage brachytherapy were evaluated, each receiving two fractions over 10 days. Multiparametric online MRI-guided prostate biopsy with 3D image verification of needle core locations enabled cores and suspicious tumor volumes to be mapped onto T2 MRI. The GTV was defined as the shared boundary of suspicious image features and malignant biopsy cores. On treatment day, radiation oncologist estimated the intended GTV boundary based on common anatomical MRI landmarks. Inverse treatment planning utilized IPSA objectives to achieve tumor V11Gy>95% and prostate V8Gy>95%, while respecting OAR constraints.

MORFEUS, a biomechanical model-based deformable image registration technique, was used to perform deformable registration of diagnostic images acquired during biopsy onto the brachytherapy planning image. Common 3D points in the prostate were identified to determine the absolute error between the observed and MORFEUS-predicted point displacements. The registered GTV was compared with the estimated GTV using Dice's coefficient and tumor D98 and V11Gy.

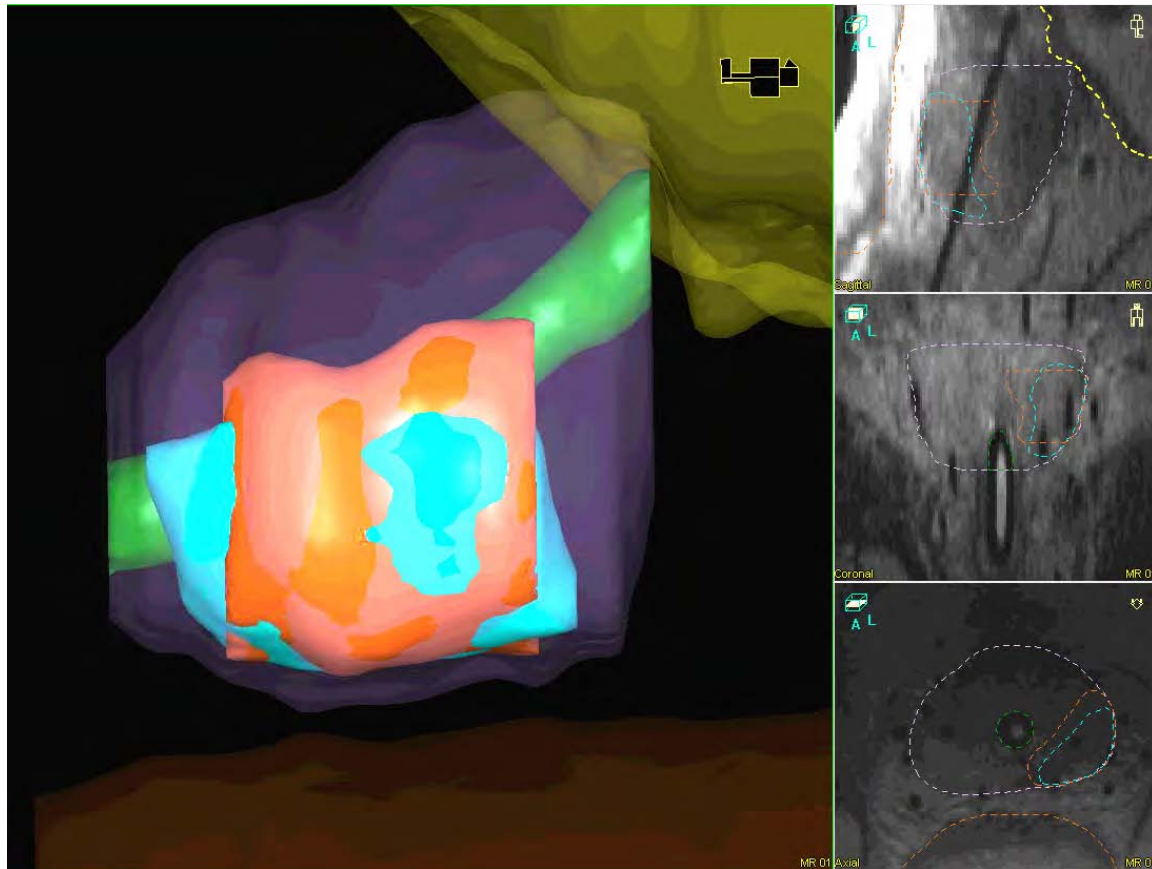
Result

The average absolute error of point displacement was 0.5mm LR, 1.3mm AP and 1.3mm SI. The average Dice's coefficient was 0.75. The majority of the geometric discrepancy occurred in

the SI dimension (Figure 1, registered and estimated GTV in blue and orange, respectively). The registered GTV received higher than intended dose in 5/7 fractions (D98 range 10.0Gy - 13.1Gy). Tumor coverage was compromised in 2/7 fractions with the estimated technique (V11Gy range 85.6% - 100%).

Conclusion

Feasibility of integrating pathologically referenced multi-parametric MRI for GTV delineation during HDR prostate brachytherapy has been demonstrated. The accuracy achieved with the deformable registration was smaller than the largest voxel dimension. A small, but potentially relevant dosimetric discrepancies between estimated and deformably registered GTV was observed. Ongoing work will explore strategies to improve AP registration accuracy, and streamline procedures to enable online use.



Clinical prostate T1 quantification using a magnetization-prepared spiral technique

Authors: Warren D. Foltz¹, Ph.D., Masoom A. Haider², M.D., Peter Chung¹, M.D., Andrew Bayley¹, M.D., Charles Catton¹, M.D., Venkat Ramanan³, David Jaffray¹, Ph.D., Graham A. Wright³, Ph.D., Cynthia Ménard¹, M.D.

Affiliations: ¹Radiation Medicine Program, Princess Margaret Hospital, University of Toronto; ²Joint Dept of Medical Imaging, Princess Margaret Hospital, University of Toronto; ³Imaging Research, Sunnybrook Hospital, University of Toronto.

Submitted to: Journal of Magnetic Resonance Imaging, Technical Note

Corresponding Author:
W. Foltz
7-301 101 College Street
Toronto, Ontario
Canada, M5G1L7
416-569-5065 (telephone)
warren.foltz@rmp.uhn.on.ca

Running title: T1prep applied to the prostate gland

Abstract

Purpose: To adapt a magnetization-prepared RF cycled spiral imaging technique, termed T₁prep, for time-efficient RF-insensitive clinical prostate T₁ quantification at 1.5 tesla, and evaluate SNR limits to voxel-based T₁ mapping.

Materials and Methods: A magnetization-prepared spiral imaging technique was adapted for robust T₁ contrast development, multi-slice imaging within 5-minutes, and data regression to a monoexponential decay. In vitro testing evaluated RF insensitivity of the multi-slice acquisition plus method accuracy. A clinical pilot study was performed in fifteen patients with low or intermediate risk localized prostate cancer.

Results: The multi-slice design displayed excellent RF insensitivity (<1% error for RF mistunings to $\pm 20\%$), and accuracy (within 0.5% of gold standard for T₁ values within 1500 ms). A clinical pilot study reported equivalence between central gland (CG) and peripheral zone (PZ) T₁ values (CG: 1321 \pm 45 ms, n=14; PZ: 1359 \pm 204 ms, n=11) and reduced tumor T₁ (1196 \pm 106 ms, p=0.028 and 0.048 compared to CG and PZ). SNR measurements identified an inappropriateness of voxel-based analysis.

Conclusions: T₁prep can quantify prostate T₁, as an adjunct measure for quantitative perfusion measurements in radiotherapy trials. Intra-patient heterogeneities support T₁ assessment within individual patients. SNR calculations will guide protocol improvements towards voxel-based analysis in future trials.

Keywords: T₁ quantification, prostate gland, quantitative MRI

Introduction

T_1 quantification is motivated primarily by a need to quantify exogenous contrast agent concentration, both from signal time-courses and for molecular targeting experiments (1). Indeed, T_1 accuracy and precision are acknowledged as principal biases for perfusion imaging analysis (2). Furthermore, endogenous T_1 retains stand-alone value, for characterization of partial oxygen pressures plus elucidation of hemorrhagic pathology (3, 4).

T_1 remains difficult to measure in vivo, despite the longevity of the field. Classical inversion-recovery approaches are prohibitively long for clinical application, while time-efficient and commercially-accessible methods assume knowledge of the radio-frequency (RF) field (5, 6). Look-Locker and variable-flip-angle standards (VFA) have demonstrated some success for biomedical translation, but the RF field must be measured independently and the flip angle reduction compromises signal-to-noise ratio (SNR) (7).

This research describes the adaption of a magnetization-prepared spiral imaging strategy for T_1 quantification of the prostate gland, termed T1prep. The method provides multi-slice coverage of the entire gland with high RF insensitivity and a clinically acceptable time-efficiency (5 minutes). A clinical pilot study involved 15 patients with newly diagnosed localized prostate cancer to evaluate zonal and tumor T_1 . SNR analysis characterized thermal noise contributions to T_1 precision, to guide protocol design for future voxel-based analysis as an adjunct measure for quantitative perfusion measurements.

Methods

All studies were performed as part of an approved prospective clinical trial. Magnetic resonance (MR) scanning was performed using a 1.5 tesla Signa (General Electric Medical Systems, Waukesha, WI).

Methodology development:

T1prep (Fig. 1) can be perceived as a time-efficient adaptation of a classical ‘single-point’ technique from T2-prepared approach (4), so that individual inversion times (TI) are sampled in sequential repetition times (TR) with robust contrast development and the entire longitudinal magnetization is sampled using a 90° excitation pulse. To achieve a clinically realistic scan time on the order of 5-minutes, spiral imaging accelerates k-space sampling and RF cycling minimizes TI sampling to 2 time-points (TI_1, TI_2).

T_1 contrast is developed using a non-selective adiabatic inversion pulse followed by an arbitrary delay of duration TI. Slice selection and spatial encoding are performed using a spectral-spatial pulse and spiral imaging gradient, with trailing spoiler gradient. Multi-slice imaging is performed by repetitive slice selection and spatial encoding at frequent intervals (~ every 20ms in different slices). A second delay of value TI' trails a final spoiler gradient. Following TI', a BIR-4 adiabatic half-passage pulse is applied to null the residual longitudinal and transverse magnetization. By preserving a constant summation of TI and TI' across variable TI, the period of longitudinal recovery is kept independent of TI selection for any TR.

Central to T1prep is RF cycling of an inversion pulse on/off on every other sequence iteration (8, 9). The difference signal is a T_1 -weighted signal decay, while the additive component of T_1 relaxation is nulled. T_1 fitting as a monoexponential decay rather than as a

monoexponential recovery provides several benefits -- TI sampling can be reduced to only 2 time points, 2-parameter fitting of a decay provides good noise performance, confusion surrounding magnetization is removed, and the measurement is inherently insensitive to imperfect inversion pulses. Because T_1 extraction from T1prep data depends on the absolute TI separation rather than absolute TI values, consistent TI values can be utilized for all slices of a multi-slice acquisition.

Quality assurance testing

Demand for reproducible tissue measures merited quality assurance testing in static phantoms.

The specific studies were as follows:

Reproducibility testing The reproducibility of the multi-slice acquisition in a static phantom was tested using a 750ml volume of water doped with manganese chloride ($MnCl_2$) placed in longitudinal orientation in a standard head coil ($T_1 \sim 610$ ms). T1prep parameter selection mapped to the proposed clinical parameterization (TI of 14 and 1014 ms, repetition time (TR) of 4400 ms, 1.1 mm resolution over a 20cm field-of-view (FOV), 6 mm slice thickness, 2 nex, 5 minute duration). Multi-slice acquisitions were then repeated following deliberate mis-tunings of the RF amplifier to almost $\pm 30\%$. A standard double-angle approach (gradient-recalled echo, flip angles of 60 and 120°, TR = 6 seconds, 128 x 128 over 20 cm field-of-view, single-slice) validated the RF distribution (10). Measurements were repeated at all RF offsets using a standard variable-flip-angle approach (gradient-recalled-echo method, TE/TR = 4.7/11 ms, $\theta = 2^\circ, 10^\circ, 20^\circ, 30^\circ$, 4 averages) (5).

Accuracy testing T1prep accuracy was tested using seven serial dilutions of Gd-DTPA (Magnevist, Berlex Canada) in 2cc eppendorff tubes (T_1 values between 400 and 2200ms).

Samples were placed upright within an eppendorff tube rack and submerged in water heavily-doped with MnCl_2 , to alleviate susceptibility effects at the air interfaces. T_1 prep was applied with the following parameters (TI = 14, 414, 814, 1214, 1614, and 2014 ms; TR = 6000 ms; 90° flip angle; 12 10.4-ms spiral interleaves at 125 kHz readout bandwidth over a 16cm field-of-view for 1.1mm in-plane resolution; 2 min 54 sec per TI value). A vendor-standard inversion-recovery spin-echo sequence provided comparative gold standard quantification (TE=10 ms, TI = 50, 400, 800, 1200, 1600, 2000, and 4000 ms, 128x128 matrix over 18 cm, 50% k-space acquisition, between 10.5 and 14.5 minutes per TI). TR was incremented to maintain a constant TR and TI difference of 11 seconds.

Clinical pilot study

A clinical pilot study involved 15 patients with low or intermediate risk localized prostate cancer and no history of prior therapy. The patients were accrued in an ongoing Phase 2 clinical trial designed to evaluate the impact of integrating MRI and advanced image-guidance towards reducing toxicity and improving quality of life after high dose intensity modulated radiotherapy. At least 3 days after ultrasound guided insertion of three-intraprostatic gold fiducial markers, all patients were scheduled for MRI of the pelvis.

Patients were positioned in supine position on the MRI table with a torso-phased array coil (MEDRAD ATD torso device, Warrendale, PA) positioned anteriorly and superiorly to the prostate gland. Scanning as a series of axial acquisitions proceeded, including anatomical fast-spin-echo imaging of the prostate region (TE/TR = 96/5000 ms, 320x256 matrix over 20 cm), diffusion-weighted echo-planar imaging (TE/TR = 64/5575 ms, 128x128 matrix over 20 cm, 6mm slices, b-values of 0 and 600 s/mm^2), and quantitative T_1 mapping (TI = 14, 1014 ms, TR =

4400 ms, 1.1x1.1mm resolution over a 20cm FOV, 6 mm slice thickness, 2 nex, 5 minute duration). A stack of up to twelve slices provided full gland coverage (72 mm).

Data analysis

Quality Assurance In vitro analysis was performed using eFilm (Merge Healthcare, Milwaukee, WI), with ROIs drawn on signal images rather than on parametric maps. T1 fitting to a monoexponential decay used Origin software (OriginLab Corporation, Northampton, MA). Origin software was also utilized for linear regression in variable-flip-angle measurements of T₁. Testing of methodological accuracy used standard Bland-Altman methodology. Algebraic tasks were performed using Matlab (The Mathworks, Natick, MA).

Prostate T₁ characterization Data analysis involved regions-of-interest (ROIs) corresponding to the central gland (CG), uninvolved peripheral zone (PZ), and tumor-dense bearing regions, delineated as hypointensities on diagnostic fast-spin echo images and apparent diffusion maps by an experienced radiation oncologist using mipav (National Institutes of Health, Bethesda, MD, USA). The urethra and intra-prostatic fiducial markers were excluded from ROIs. ROIs were applied to T1prep signal images and manually corrected to account for evident motion. T₁ fitting used Origin software. Signal-to-noise (SNR) calculations used the methods of Constantinides et al, for phased-array coil acquisitions (11).

Results:

Quality assurance

Using a centrally-placed ROI in each of ten 6-mm thick slices, T1prep preserved the T_1 standard deviation of the multi-slice acquisition well within 1% for RF offsets between $\pm 25\%$ (Fig. 2(a, b)). Comparatively, T_1 error for a standard VFA approach increased by approximately 20% for every 10% offset of the RF field. T1prep also demonstrated excellent agreement with the gold-standard inversion recovery approach (Fig. 2(c, d)). Across all data points, Bland-Altman bias and limits of agreement were 37 and 169 ms. However, the analysis suggested an increasing disagreement between measurements as sample T_1 approached 2000 ms. T_1 agreement was within 27 ms (i.e. 0.5%) for T_1 values of 1500 ms or less.

Clinical pilot study – Prostate T_1 quantification

Representative axial T1prep images of the prostate gland at base, mid, and apical locations are presented in Fig. 3. Figure 4 displays T_1 maps through tumor-bearing regions of the peripheral zone, plus supporting diagnostic ADC maps and FSE images.

From clinical acquisition, the mean zonal T_1 values were equivalent at 1321 ± 45 ms ($n = 14$) and 1359 ± 204 ms ($n = 11$) for CG and PZ respectively ($p = 0.50$). Inter-patient T_1 heterogeneity was significant, with individual ROIs ranging in T_1 from 1237 to 1381 ms for CG, and from 1060 to 1778 ms for PZ. T_1 values in tumor-dense ROIs were 1196 ± 106 ms (minimum: 1040 ms; maximum: 1335 ms, $n = 8$). Tumor T_1 were significantly shorter than both CG T_1 (difference = 116 ± 118 ms, $p = 0.0276$) and PZ T_1 (difference = 179 ± 212 ms, $p = 0.0484$) (Fig. 4).

From histogram analysis, 95% of the delineated voxels presented with SNR values of 32 (CG) and 29 (PZ) or more at TI_1 . At TI_2 , 95% of SNR values were greater than 15 for CG and 13 for PZ so that T_1 estimates were effectively unbiased by the noise baseline in magnitude images.

Discussion

This research provides a novel technical solution for the challenging problem of RF-insensitive and time-efficient quantitative prostate T_1 measurements. The method leverages the robust contrast generation of a non-selective adiabatic inversion pulse, the rapid multi-slice imaging capability of spiral imaging, and RF cycling to reduce TI sampling requirements while providing an advantageous dependence between signal-to-noise and T_1 precision. Clinical investigation in patients with low and intermediate risk prostate cancer demonstrated equivalence between CG and prostate T_1 , and a significantly reduced tumor T_1 . SNR analysis identified a minimum-useful sampling volume for thermal-noise insensitive T_1 quantification, and identified SNR requirements for future trials planning voxel-based analysis.

The T1prep design has similarities to the RF pulse train approaches of Hsu and co-workers because RF cycling is used to minimize the additive contribution to T_1 relaxation (8, 9). However, Hsu samples the resultant T_1 decay with a train of RF pulses with reduced RF flip angle, while the RF pulse train in T1prep is utilized for multi-slice imaging and a 90° flip angle is retained to maximize SNR in each slice. The method may not be as rapid as published applications of quantitative T_1 strategies using variable-flip-angle (VFA, DESPOT1), inversion-recovery with ssfp readout (ir-ssfp), and look-locker echo-planar imaging (LL-EPI) (5, 7, 12, 13). However, methodology comparisons are constrained by the predominant neurology focus of these trials, where the superb sensitivity of current head coils can be leveraged for scan time reduction. In addition, variable-flip-angle and ssfp-based techniques are inherently sensitive to RF field heterogeneity, which necessitates independent RF field mapping (5). The most relevant

existing comparison may be the application by Kershaw et al of a 3D-inversion recovery turbo field echo technique for prostate evaluation at 1.5 tesla, achieving 2x2x5 mm interpolated voxels within a 4-minute scan time though representative images were not provided (14).

The high RF insensitivity of the T1prep technique should be a particular strength of the design, and should have increasing value as higher field strength applications are developed. In comparison, a standard VFA approach with flip angles of 2°, 9°, and 19° would introduce T₁ biases of approximately ±20 and ±40% at RF offsets of ±10 and ±20%, while T1prep maintains T₂ biases on the order of 1% or less over a similar range of RF mis-tuning.

Prostate T₁ characterization Prostate T₁ quantification seems to be sparsely covered in the literature, and existing publications seem to have reasonable to very good agreement with the current results. Noteworthy is Kjaer's early application of an inversion-recovery approach with 6 inversion times at 1.5 T (15). He identified T₁ values of 1022 ms for normal prostate tissue and 1050 ms for carcinoma. Similarly, Kershaw et al measured T₁ using a variable-flip-angle approach and identified an equivalent normal prostate and adenocarcinoma T₁ in 21 patients (normal prostate: 922 ms (692 – 1130 ms); tumor: 916 ms (795 – 1172 ms)) (16). More recently, Kershaw et al. identified median central gland and peripheral zone T₁ values of 1390 and 1360 ms at 1.5 tesla, in patients with benign prostatic hyperplasia and an absence of prostate cancer. The intra-quartile ranges were approximately 10% (14). In a prior study, DeBazelaire et al. measured mean and standard deviation prostate gland T₁ values of 1317±85 ms at 1.5 tesla and 1597±42 ms at 3.0 tesla using matched regions-of-interest (17). Noworolski et al. quantified prostate T₁ values at 1.5 T using a spin-echo method at up to four repetition times, and reported T₁ of 1570±622 ms for normal peripheral zone and 1670±421 ms for peripheral zone cancer (18).

SNR analysis SNR estimates are significant because they define the best case precision of the T_1 measurement. Based on Monte Carlo simulation, a monoexponential decay at experimental TI and T_1 of 1300 ms identifies a noise-mediated T_1 standard deviation (σT_1) of 5%, 2.5%, 2%, 1.5%, and 1% at SNR values of 35, 70, 90, 115, and 170. σT_1 for fitting a 2-parameter monoexponential recovery with 3 TI and equivalent T_1 and SNR is similar, but care must be taken to judge the polarity of small magnitude signals.

Using T1prep, histogram analysis reported a SNR of 32 or more in at least 95% of voxels at TI_1 , so that voxel-based analysis would be prone to variability from thermal noise ($\sigma T_1 \sim 5\%$ at SNR of 35). One may then combine voxels into a ROI to increase robustness to thermal noise, and the SNR gain is proportional to the square root of the number of independent voxels within the ROI. For example, combination of 10 voxels (i.e. 73 mm^3 sampling volume) with SNR 30 would maintain thermal noise variability within 2%, while a 35 voxel ROI (254 mm^3 sampling volume) would maintain thermal noise variability within 1%. Consequently, noise precision is traded off for volume averaging in the absence of other strategies to augment SNR.

It is worthwhile to note that TI selection can be tailored for the target T_1 . Roughly, to maximize precision of monoexponential fitting using two data-points only, TI_1 should be minimized while TI_2 should be 1.1 times the expected time-constant (19). For this pilot trial, TI_2 was 1014 ms so that an incremental increase in noise performance could be gained via prolongation of TI_2 towards 1400 ms at experimentally measured T_1 . Slice number may need to be constrained for contrast-enhanced studies because T_1 decay during the imaging interval may limit SNR independently of TI selection.

Clinical significance The primary clinical significance of T_1 quantification is its central role as an adjunct measure for quantitative analysis of dynamic contrast enhancement (DCE) (2, 20). These results highlight a considerable intra-patient zonal and T_1 heterogeneity which further supports individual T_1 assessment in DCE examinations. Ideally, a progression of dynamic prostate evaluation to voxel-based analysis will be concomitant with a progression of quantitative T_1 evaluation within registered voxels. Part and parcel of this progression to voxel-based parametric mapping will be a growing importance of thermal noise variability, particularly for regression analysis with sparse samples (i.e. ADC, T_1 , T_2). Practical solutions for measurements with noise-limited precision at constant voxel volume and scan time include improved RF configurations (i.e. endo-rectal coils in tandem with torso phased-arrays) and stronger magnets.

Conclusions

A magnetization-prepared spiral imaging strategy has been adapted for time efficient and RF-insensitive prostate T_1 quantification. Applied to patients with low or intermediate risk localized prostate cancer and no treatment history, it demonstrated equivalence between mean zonal T_1 values and a reduced tumor T_1 . However, intra-patient zonal and tumor T_1 heterogeneities were considerable so that individual prostate T_1 mapping is merited for quantitative assessment of contrast enhancement dynamics. SNR analysis identified constraints for thermal noise insensitive T_1 measurements, to guide protocol design for voxel-based T_1 quantification as an adjunct measure to support voxel-based DCE analysis.

References:

1. Tofts P. Modeling tracer kinetics in dynamic Gd-DTPA MR imaging. *J Magn Reson Imaging* 1997;7:91-101.
2. Dale B, Jesberger J, Lewin J, Hillenbrand C, Duerk J. Determining and optimizing the precision of quantitative measurements of perfusion from dynamic contrast enhanced MRI. *J Magn Reson Imaging* 2003;18:575-584.
3. Tadamura E, Hatabu H, Li W, Prasad P, Edelman R. Effect of oxygen inhalation on relaxation times in various tissues. *J Magn Reson Imaging* 1997;7:220-225.
4. Foltz W, Yang Y, Graham J, Detsky J, Wright G, Dick A. MRI relaxation fluctuations in acute reperfused infarction. *Magn Reson Med* 2006;56:1311-1319.
5. Cheng H, Wright G. Rapid high-resolution T1 mapping by variable flip angles: Accurate and precise measurements in the presence of radiofrequency field inhomogeneity. *Magn Reson Med* 2006;55:566-574.
6. Crawley A, Henkelman R. A comparison of one-shot and recovery methods in T1 imaging. *Magn Reson Med* 1988;7:23-34.
7. Deichmann R. Fast High-resolution T1 mapping of the human brain. *Magn Reson Med* 2005;54:20-27.
8. Hsu J, Zaharchuk G, Glover G. Rapid methods for concurrent measurement of the RF-pulse flip angle and the longitudinal relaxation time. *Magn Reson Med* 2009;61:1319-1325.
9. Hsu J, Glover G. Rapid MRI method for mapping the longitudinal relaxation time. *J Magn Reson* 2006;181:98-106.

10. Cunningham C, Pauly J, Nayak K. Saturated double-angle method for rapid B1+ mapping. *Magn Reson Med*. 2006;55:1326-1333.
11. Constantinides C, Atalar E, McVeigh E. Signal-to-noise measurements in magnitude images from NMR phased arrays. *Magn Reson Med* 1997;38:852-857.
12. Scheffler K, Henning J. T1 Quantification with Inversion Recovery TrueFISP. *Magn Reson Med* 2001;45:720-723.
13. Deoni S, Peters T, Rutt B. High-resolution T1 and T2 mapping of the brain in a clinically acceptable time with DESPOT1 and DESPOT2. *Magn Reson Med* 2005;53:237-241.
14. Kershaw L, Hutchinson C, Buckley D. Benign prostatic hyperplasia: Evaluation of T1, T2, and microvascular characteristics with T1-weighted dynamic contrast-enhanced MRI. *J Magn Reson Imaging* 2009;29:641-648.
15. Kjaer L, Thomsen C, Iversen P, Henriksen, O. In vivo estimation of relaxation processes in benign hyperplasia and carcinoma of the prostate gland by magnetic resonance imaging. *Magn Reson Imaging* 1987;5:23-30.
16. Kershaw L, Logue J, Hutchinson C, Clarke N, Buckley D. Late tissue effects following radiotherapy and neoadjuvant hormone therapy of the prostate measured with quantitative magnetic resonance imaging. *Radiother Oncol* 2008;88:127-134.
17. de Bazelaire C, Duhamel G, Rofsky N, Alsop D. MR imaging relaxation times of abdominal and pelvic tissues measured in vivo at 3.0 T: Preliminary results. *Radiology* 2004;230:652-659.
18. Noworolski S, Henry R, Vigneron D, Kurhanewicz J. *Magn Reson Med* 2005;53:249-255.
19. Kurland R. Strategies and tactics in NMR relaxation time measurements. I. Minimizing relaxation time errors due to image noise -- the ideal case. *Magn Reson Med* 1985;2:136-158.

20. Cheng H. T1 measurement of flowing blood and arterial input function determination for quantitative 3D T1-weighted DCE-MRI. *J Magn Reson Imaging* 2007;25:1073-1078.

Figure Legends:

Figure 1: T1prep pulse sequence design. T_1 contrast is developed globally during a preparation interval of duration TI , termed the inversion time. Multi-slice imaging is performed using a spectral-spatial pulse and spiral imaging gradients, applied repetitively for each imaging slice ('N' times for 'N' slices). Following a duration TI' , an adiabatic BIR-4 pulse is applied to null the remnant longitudinal magnetization. Measurement independence on the TR is achieved by maintaining a consistent summed $TI + TI'$ for all inversion times. On every other sequence iteration, RF cycling of a second adiabatic inversion pulse is applied prior to the start of the imaging interval to null the additive T_1 recovery term.

Figure 2: Quality Assurance testing: (a) Reproducibility phantom, displaying B1 map along a coronal section of a $MnCl_2$ -doped water bottle phantom (long rectangle), and location of 10 imaging slices plus approximate diameter of ROIs in T1prep images (short parsed rectangle); (b) Percentage T_1 error as a function of RF offset, demonstrating negligible RF sensitivity using multi-slice T1prep and considerable RF sensitivity using a variable-flip-angle approach; (c) T1prep images of an accuracy phantom, consisting of 7 eppendorff tubes doped to variable extent with Gd-DTPA, and oriented vertically in a bath of water heavily doped with $MnCl_2$; (d) Bland-Altman analysis demonstrating equivalence between T1prep and the gold standard inversion-recovery technique. The bias and limit of agreement (LOA) are displayed.

Figure 3: Representative clinical images at three levels of the prostate gland: (top row; a-c) standard diagnostic FSE sections; (middle row; d-f) TI_1 T1prep images; (bottom row; g-i) TI_2

T1prep images. Implanted gold intra-prostatic fiducial marker are visible as focal hypointensities in in each spiral image.

Figure 4 – Representative images from three patients, termed patients A, B. and C; (left) ADC map; (mid) diagnostic FSE image; and (right) quantitative T_1 maps (windowed between 0 and 2000ms). For each cases, hypo-intense regions deemed to be tumor-dense can be visualized in both ADC and FSE acquisitions. Patient A displayed T_1 values of 1272 ms (CG), 1349 ms for peripheral zone, and 1162 ms for tumor. Patient B displayed T_1 values of 1329 ms (CG), 1311 ms for peripheral zone, and 1174 ms for tumor.

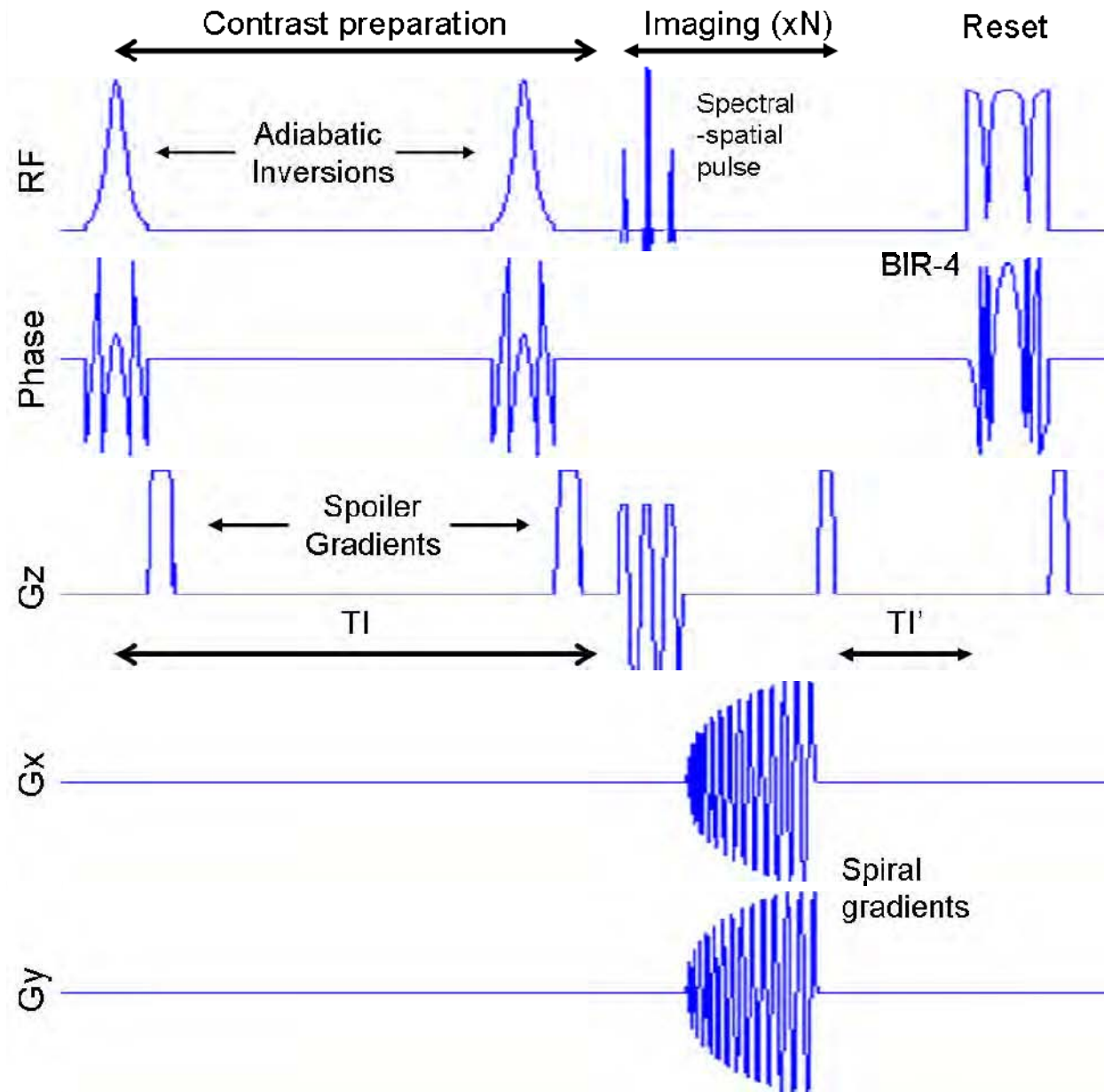


Figure 1: T₁prep pulse sequence design. T₁ contrast is developed globally during a preparation interval of duration TI, termed the inversion time. Multi-slice imaging is performed using a spectral-spatial pulse and spiral imaging gradients, applied repetitively for each imaging slice ('N' times for 'N' slices). Following a duration TI', an adiabatic BIR-4 pulse is applied to null the remnant longitudinal magnetization. Measurement independence on the TR is achieved by maintaining a consistent summed TI + TI' for all inversion times. On every other sequence

iteration, RF cycling of a second adiabatic inversion pulse is applied prior to the start of the imaging interval to null the additive T_1 recovery term.

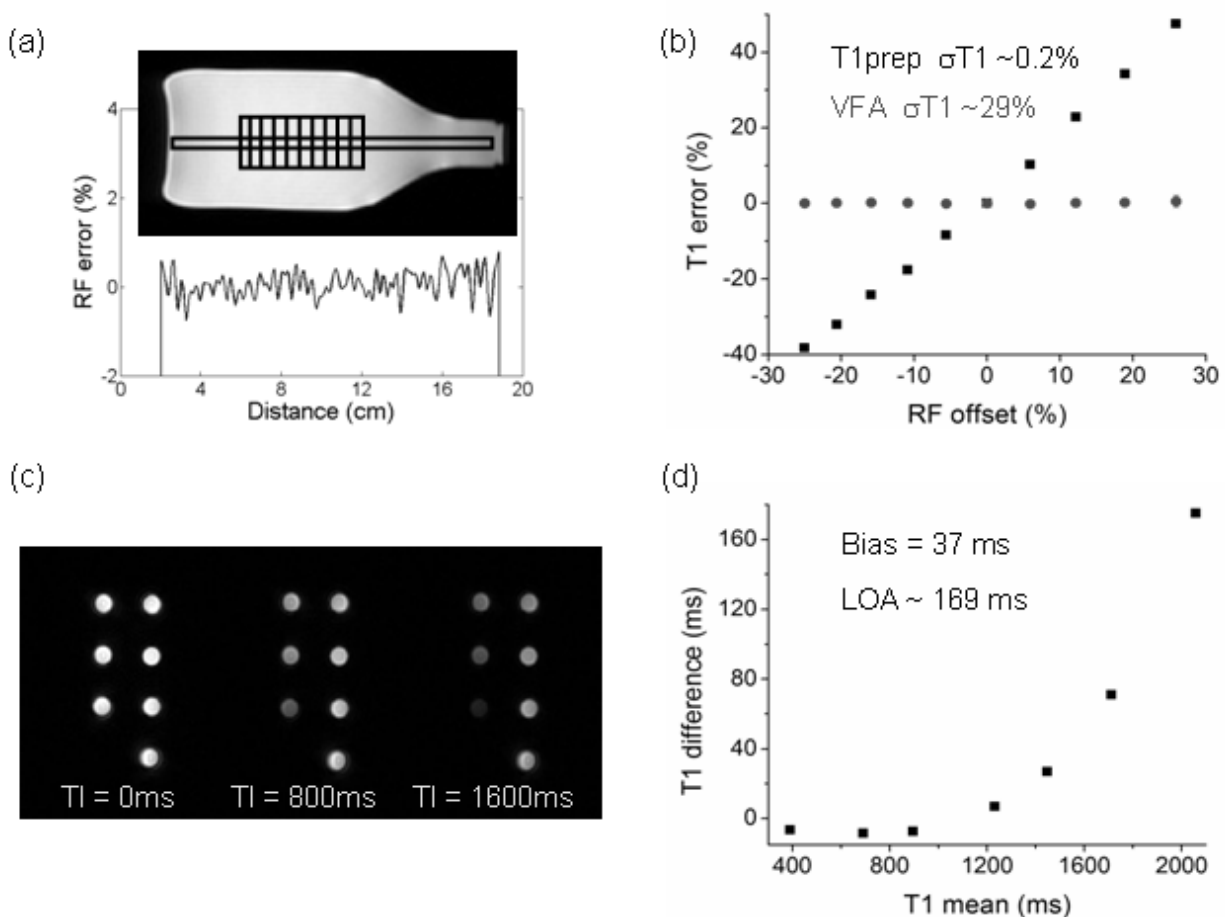


Figure 2: Quality Assurance testing: (a) Reproducibility phantom, displaying B1 map along a coronal section of a MnCl₂-doped water bottle phantom (long rectangle), and location of 10 imaging slices plus approximate diameter of ROIs in T1prep images (short parsed rectangle); (b) Percentage T₁ error as a function of RF offset, demonstrating negligible RF sensitivity using multi-slice T1prep and considerable RF sensitivity using a variable-flip-angle approach; (c) T1prep images of an accuracy phantom, consisting of 7 eppendorff tubes doped to variable extent with Gd-DTPA, and oriented vertically in a bath of water heavily doped with MnCl₂; (d) Bland-Altman analysis demonstrating equivalence between T1prep and the gold standard inversion-recovery technique. The bias and limit of agreement (LOA) are displayed.

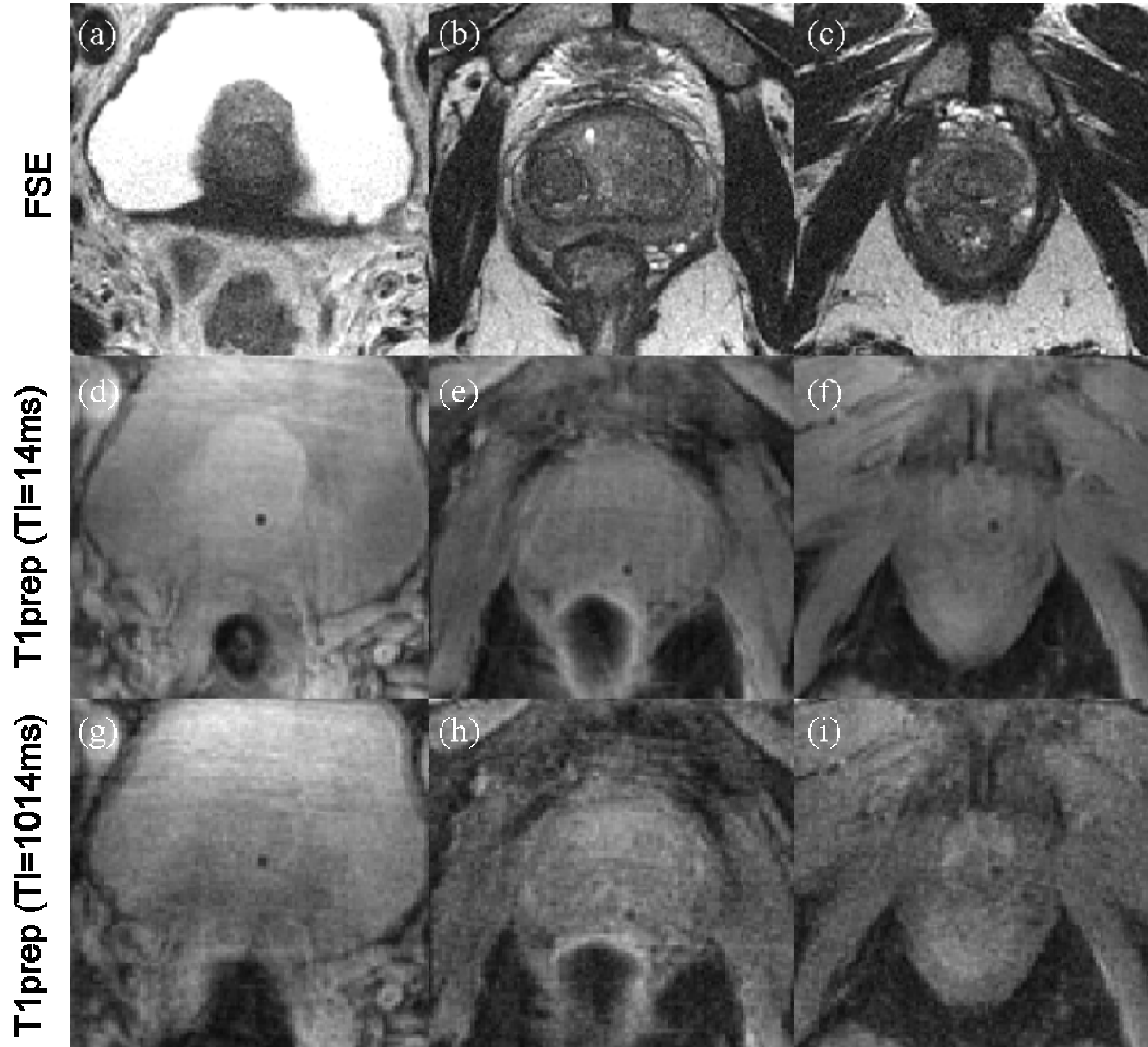


Figure 3: Representative clinical images at three levels of the prostate gland: (top row; a-c) standard diagnostic FSE sections; (middle row; d-f) $T1_1$ T1prep images; (bottom row; g-i) $T1_2$ T1prep images. Implanted gold intra-prostatic fiducial marker are visible as focal hypointensities in in each spiral image.

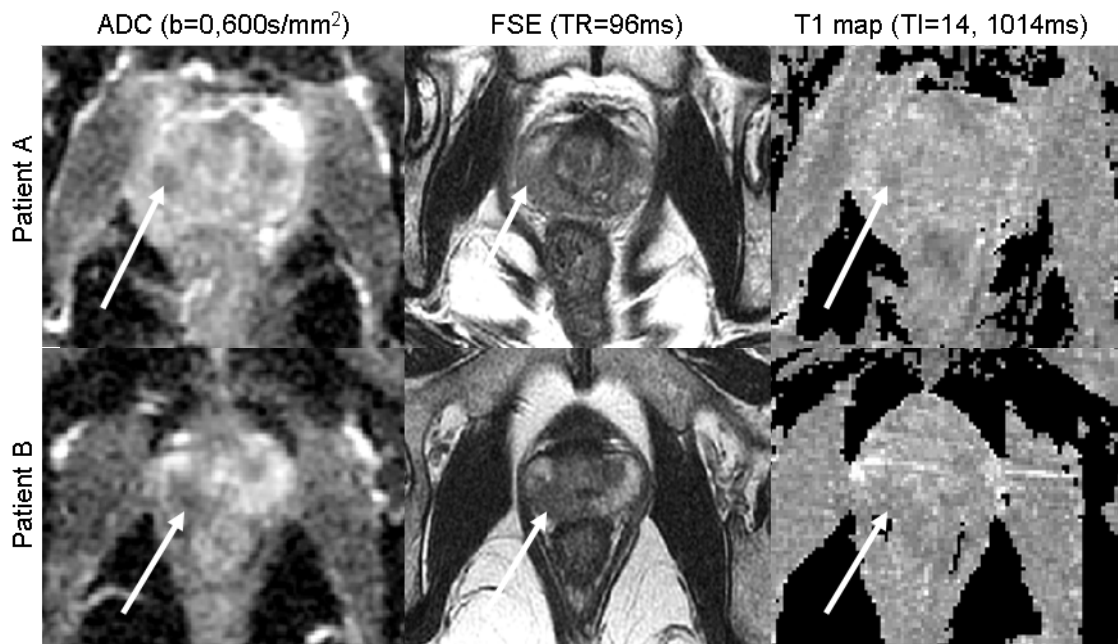


Figure 4 – Representative images from three patients, termed patients A, B. and C; (left) ADC map; (mid) diagnostic FSE image; and (right) quantitative T_1 maps (windowed between 0 and 2000ms). For each cases, hypo-intense regions deemed to be tumor-dense can be visualized in both ADC and FSE acquisitions. Patient A displayed T_1 values of 1272 ms (CG), 1349 ms for peripheral zone, and 1162 ms for tumor. Patient B displayed T_1 values of 1329 ms (CG), 1311 ms for peripheral zone, and 1174 ms for tumor.

Clinical prostate T₂ quantification using magnetization-prepared spiral imaging

Authors: Warren D. Foltz¹, Ph.D., Supriya Chopra¹, M.D., Peter Chung¹, M.D., Andrew Bayley¹, M.D., Charles Catton¹, M.D., David Jaffray¹, Ph.D., Graham A. Wright³, Ph.D., Masoom A. Haider², M.D., Cynthia Ménard¹, M.D.

Affiliations: ¹Radiation Medicine Program, Princess Margaret Hospital, University of Toronto; ²Joint Dept of Medical Imaging, Princess Margaret Hospital, University of Toronto; ³Imaging Research, Sunnybrook Hospital, University of Toronto.

Submitted to: Magnetic Resonance in Medicine, Technical Note

Corresponding Author:
W. Foltz
7-301 101 College Street
Toronto, Ontario
Canada, M5G1L7
416-569-5065 (telephone)
warren.foltz@rmp.uhn.on.ca

Word count: 2461

Running title: Clinical prostate T₂ quantification using spiral T₂prep

Abstract

T_2 quantification may augment diagnostic T_2 -weighted imaging; to improve cancer detection via auto-segmentation of multi-parametric acquisitions and to potentiate longitudinal studies of prostate cancer. However, robust quantitative techniques are not generally accessible or refined for clinical translation. This research describes the adaptation of a magnetization-prepared spiral imaging technique, termed T2prep for prostate application, providing whole gland coverage within a 5-minute interval with considerable insensitivity to radio-frequency (RF) inhomogeneities. Clinical piloting in two cohorts with distinct clinical histories demonstrated the anticipated differences in zonal and tumor T_2 , including tumor T_2 shortening compared to peripheral zone, and post-radiotherapy shortening of peripheral zone T_2 . SNR calculations were performed for data acquired with or without an endo-rectal coil in tandem with a torso phased array, to judge the potential for voxel-based T_2 mapping and thereby support focal biological characterization of cancer, hypoxia, and response to therapy within regions of dense cancer burden.

Introduction

Quantitative MRI biomarkers (i.e. apparent diffusion coefficient, vascular metrics, metabolite profiles) are particularly relevant for cancer management, both for differential diagnosis and to judge the efficacies of novel therapeutic strategies over time in pre-clinical and clinical trials (1). T_2 relaxation is also central to MRI diagnostics, and T_2 quantification may complement both diagnostics and trials of tumor response (2-4). However, T_2 quantification is often restricted to research purposes despite the long and rich history of MR relaxometry.

Robust T_2 quantification in vivo constrains pulse sequence design to limit biases from system imperfections and mis-tunings, physiologic motions, and volume averaging, without compromising time-efficiency and volumetric coverage targets (5, 6). Within this paradigm, a magnetization-prepared spiral imaging technique, termed T2prep, was refined to provide an imaging solution for vascular oximetry measurements and peripheral venous angiography, though characteristics of robust global contrast development and longitudinal storage of contrast also support quantitative tissue evaluation (7, 8).

This paper describes an adaption of T2prep for clinical prostate measurements to quantify zonal and tumor T_2 and SNR values. Clinical piloting used two patient cohorts, which are distinct based on patient history of radiotherapy and on inclusion of an endo-rectal coil for MR signal reception. SNR analysis estimated noise precision in voxel-based maps, to guide protocol design for future evaluation of hypoxia and therapy response.

Methods

All patients provided informed consent and were prospectively enrolled in approved clinical trials. All studies were performed using a 1.5 tesla MRI scanner (Signa, General Electric Medical Systems, Waukesha, WI).

Patient selection

Cohort A

Cohort A included 16 men with low/intermediate risk localized prostate cancer and accrued in an ongoing Phase 2 clinical trial. At least 3 days after ultrasound guided insertion of three intraprostatic gold fiducial markers, all patients were scheduled for radiation planning CT scanning (2mm axial cuts, no spacing) followed by MRI of the pelvis.

Cohort B

Cohort B included 8 men suspected to have local recurrence following external beam radiotherapy and accrued in an ongoing clinical trial of MRI guided biopsy for evaluation of local recurrence.

T2Prep acquisition method

Figure 1 presents the template for the T2prep technique (5-8). T_2 contrast is prepared using a non-selective robust refocusing train, returned to the longitudinal axis. Slice selection and spatial encoding are performed using a spectral-spatial pulse and spiral imaging gradient, with trailing spoiler gradient. Multi-slice imaging is performed by repetitive slice selection and spatial encoding at frequent intervals (~ every 20ms in different slices). A BIR-4 adiabatic half-passage pulse trails the final imaging interval to null the residual longitudinal and transverse

magnetization. The delay between the spiral readout and BIR-4 pulse is shifted to keep the period of longitudinal recovery independent of TE for the interleaved acquisition. RF cycling is applied, consisting of an adiabatic inversion pulse prior to the first imaging interval of every other sequence iteration. Subtraction isolates the T_2 -weighted decay function without bias from additive T_1 relaxation during the period of longitudinal storage.

Experiment 1: Quality Assurance

Quality testing evaluated the RF sensitivity of the multi-slice T2prep acquisition, using a 750 ml bottle of MnCl₂-doped water ($T_2 \sim 72$ ms), the head coil of the GE Signa, and a 12-slice prescription covering 7.2 cm in 6-mm sections. The T2prep parameter set included 2 echo times (TE) of 3.2 and 88.4 ms, 4400 ms repetition time (TR), 1.1x1.1x6-mm voxels based on spiral k-space sampling at 125 kHz over a 20-cm field-of-view, and 2 averages for a 5-minute scan duration. RF tuning was validated using the double-angle technique (gradient-recalled echo acquisitions at flip angles of 60 and 120° with minimized echo times of 1.3 ms, long repetition times of 8500 ms, and 128x64 matrix over a 20 cm field-of-view) (9). The B_1 profile was calculated after averaging 10 adjacent voxels at each point along the length of the phantom. The T2prep acquisition was repeated at 5 unit increments of the RF amplifier (ranging from ± 20 %) via deliberate system mis-tunings, to encompass the characteristic ± 15 % offsets of a 1.5 tesla whole-body scanner (7).

Experiment 2: T_2 quantification in patients with low or intermediate risk localized prostate cancer prior to external beam radiotherapy

Cohort A patients were positioned supine on the MRI table with a torso-phased array coil (MEDRAD ATD torso device, Warrendale, PA) placed anterior and posterior to the pelvis. The MRI examination proceeded, as a series of axial scans of the prostate with fixed graphical prescription and common 20 cm field-of-view, including 2D-FSE imaging (TE/TR = 96/5000 ms, echo-train length = 16, 320x256 matrix, 3 mm slice thickness), diffusion-weighted echo-planar imaging (TE/TR=64/5575 ms; b = 0 and 600 s/mm², 128x128 matrix, 6 mm slice thickness), and T2prep (TE = 3.2, 88.4 ms; TR= 4400 ms, 1.1x1.1 mm voxels, 6 mm slice thickness, 5 minute scan). The majority of acquisitions required 10 to 12 6-mm slices for full prostate coverage.

Experiment 3: T2 quantification in patients with suspected local recurrence after external beam radiotherapy

Cohort B patients were positioned supine on the MRI table and an endorectal coil (MEDRAD MRInnervu endorectal coil) - modified to attach to a locking device, was inserted. A pelvic phased array coil (MEDRAD ATD torso device) was positioned anterior and posterior to the pelvis. T2prep (TE = 3.2, 88.4 ms; TR= 4400 ms, 1.1x1.1x6 mm voxels over a 20 cm field-of-view, 5 minute scan, 10-12 slices for typical whole gland coverage) was then incorporated into a multi-parametric MRI protocol, which included 2D-FSE and DW-EPI. The latter acquisitions shared similar parameters with the design of Experiment 2.

Data analysis

For experiment 1, the RF field was mapped via standard analysis of the double-angle method (Matlab, The Mathworks, Natick, MA) (9). Echo time and signal magnitude data pairs were

extracted using contours drawn on eFilm (Merge Healthcare, Milwaukee, WI). T₂ regression analyses were performed using the Origin software package (OriginLab, Northampton, MA).

For experiments 2 and 3, signal magnitudes were extracted from regions-of-interest (ROIs) representing the central gland (CG) and peripheral zone (PZ), which were delineated manually using MIPAV® (NIH version 4.2.1) on FSE images by an experienced radiation oncologist. Tumor ROIs were demarcated on FSE images, guided by visualization of characteristic nodular hypointensities in diffusion-weighted and/or FSE images, rapid and intense contrast enhancement and washout on DCE, and needle core biopsy results. FSE ROIs were copied onto T₂prep images, and manually adjusted to account for motion-related mis-registration and to exclude artifacts of implanted gold seeds. Signal-to-noise for a given ROI was calculated as per methods of Constantinides et al, for phased-array coil acquisitions (10). All significance testing used the Student's two-tailed t-test, with significance defined by reduction of the p-value below 0.05.

Results

Experiment 1: Quality Assurance

Figure 2(a) displays the RF uniformity along the MnCl₂-doped water phantom, as demarcated by the solid line. The dashed box demarcates approximately the prescription of the 12-slice acquisition plus centrally-placed ROIs. Within this volume, the RF amplitude remained within 0.2 % of the target amplitude. Figure 2(b) displays the mean and standard deviation of T₂ across all slices at a given RF offset, using a centrally placed ROI of 3cm². The T₂ offset remains well within 2 % for RF offsets of 10 % or less, but elevates towards 3 % for RF offsets of 15%. T₂

error accrues more rapidly at RF offsets of 15 % or greater, consistent with the limits for success of the MLEV pattern of 90x180y90x composite refocusing pulses (6).

Experiment 2: T₂ quantification in patients with low or intermediate risk localized prostate prior to external beam radiotherapy

Figure 3 displays representative T₂prep images and corresponding T₂ maps across base, mid, and apical regions of the prostate. The locations of gold intra-prostatic fiducial markers are displayed as focal hypointensities in the proton-density-weighted images.

Zonal T₂ values were 78±7 ms for CG and 109±25 ms for PZ (p = 0.0002). Peripheral zone tumors were identified in 11 of 16 subjects. At a mean of 81±10 ms, tumor T₂ was reduced significantly from uninvolved peripheral zone by 30±24 ms (range: 9 to 91 ms, p = 0.0026). From histogram analysis, 95% of the delineated voxels in zonal ROIs presented with SNR values of 28 (CG) and 27 (PZ) or more, at the first TE of 3 ms. The corresponding lower confidence intervals for SNR at the second TE of 88ms were approximately 9 for both CG and PZ.

Experiment 3: T₂ quantification in patients with suspected local recurrence after external beam radiotherapy

Representative T₂-weighted images and T₂ maps at basal, middle, and apical regions of the prostate gland are illustrated in Fig. 4. A comparison of Cohort A and B images in tumor-bearing regions are presented in Fig. 5. Artifacts of the patient preparation included a bright intra-urethral signal due to foley catheterization (3/8 patients) and occasional intra-prostatic edema from injection of local anesthetic (5/9 patients). These regions were excluded from ROIs.

The mean T_2 values were 72 ± 6 ms for the CG, and 94 ± 12 ms for the PZ ($p = 0.003$, $n = 8$). Tumor-dense regions were identified in 5 of 8 subjects (Fig. 5(b)). The mean tumor T_2 was 81 ± 4 ms, which approached significance in difference with the uninvolved PZ ($p=0.08$, $n=5$). Consistent with the sensitivity profile of the endo-rectal coil, histogram analysis identified a non-normal distribution of image SNR, so that voxels had mean and standard deviation SNRs of 96 ± 21 for CG and 147 ± 32 for PZ, but 95% of the CG voxels had SNR greater than 62 and 95% of PZ voxels had SNR greater than 98.

Discussion

This research describes the adaptation of a T_2 -prepared spiral imaging method for T_2 quantification in prostate radiotherapy. The method effectively combines RF insensitivity with time-efficiency and multi-slice coverage. Clinical piloting used two cohorts at distinct stages of cancer progression and radiation treatment. Our results are consistent with the known variations in prostate T_2 , including elevated values in PZ compared to CG and tumor, and reduced prostate T_2 contrast following external beam irradiation. Specifically, Cohort B presented with lower PZ T_2 at near-equivalent CG and tumor T_2 compared to Cohort A. SNR analysis characterized the potential for voxel-based T_2 mapping when a torso phased array coil is used with and without an endo-rectal coil. This standard is a step in the progression towards robust voxel-based T_2 mapping

Technical relevance

Motivation to review T_2 measurement development is a surprisingly broad divergence in prostate measurements. Divergent results may stem from the lack of a standardized technique, including factors affecting robustness and echo time sampling, given accumulating evidence of non-monoexponential prostate T_2 relaxation (11, 12). For example, Gibbs et al demonstrated zonal T_2 of 88 ± 13 ms (CG) and 122 ± 34 ms (PZ) and sampled to 112 ms (2), Langer et al demonstrated PZ and tumor T_2 of 108 and 82 ms and sampled to 90 ms (4), Kershaw et al demonstrated median CG and PZ T_2 on the order of 150 ms and sampled to 240 ms (13), while Roebuck et al demonstrated suspected healthy and suspected cancer T_2 values of 193 ± 49 ms and 100 ± 26 ms and sampled to 180 ms (14). Current results are consistent in TE selection and T_2 to Langer et al (4).

In design, T2prep presents with advantages over the standard Carr-Purcell-Meiboom-Gill (CPMG) refocusing train, because it uses a validated combination of non-selective refocusing pulses and scan time does not limit slice coverage. However, scan time increases linearly with the number of echo times, which constrains T_2 fitting to a monoexponential decay if only 2 echo times are acquired. This paper presented a 5 minute whole-gland acquisition with 7.3 mm^3 voxels. In comparison, Roebuck et al. demonstrated a 10.7-minute voxel-based T_2 mapping of the prostate gland with $0.55 \times 1.09 \times 4$ mm voxels (2.4 mm^3 volume) using a CPMG technique augmented by an endo-rectal coil in combination with a 4-coil torso phased array at 1.5 tesla (14). Kershaw et al utilized parallel imaging to reduce the data acquisition time of a CPMG approach to 4-minutes, using a cardiac phased-array coil at 1.5 tesla with 2.3 mm interpolated in-plane resolution and a 4.5 mm slice thickness (at least 23.8 mm^3 voxels) (13). However, CPMG refocusing pulses must be slice-selective to gain the time efficiency of slice-interleaving for multi-slice acquisitions, which artificially accelerates T_2 relaxation (15).

SNR

By definition, SNR defines the maximal precision for T_2 quantification. SNR analysis is therefore requisite for progression from ROI to voxel-based T_2 mapping, to support diagnostics based on auto-segmentation, biopsy guidance, tumor hypoxia quantification, and tumor radiation response quantification.

From Monte Carlo simulation of a monoexponential decay at experimental TE and T_2 of 80ms, T_2 standard deviation from thermal noise reduces below 5%, 2.5%, 2%, 1.5%, and 1% for SNR values of 35, 70, 90, 115, and 170. From histogram analysis of Cohort A, 95% of the voxels presented with SNR values of 28 (CG) and 27 (PZ) or more, at the first TE of 3 ms. Consequently, any voxel-based analysis would be quite prone to thermal noise variability. For cohort B, 95% of the voxels in zonal ROIs presented with SNR values of 62 (CG) and 98 (PZ). Consequently, voxel-based analysis of the T2prep method approaches feasibility when an endo-rectal coil is used in tandem with a torso-phased array.

At all TE values, SNR must also be significantly greater than the noise magnitude, else the T_2 estimate is artificially elevated by the noise baseline signal. For Cohort A, 95% of voxels had SNR of greater than 9 at the second TE of 88ms, so that noise bias was not significant .

Clinical relevance

T_2 -weighted imaging provides moderate sensitivity (50-77%) and specificity (36-63%) for identifying tumor-dense regions of the prostate gland, with improved diagnostic performance for combined pelvic phased array and endo-rectal coil acquisitions (77-96%) (16-17). However, diagnostic performance is reduced in patients with small tumor burden (size < 10 mm, volume < 5

ml) (17), transition zone or anterior disease (16), low tumor density (5), or prior history of external beam irradiation (18). Diagnostic performance is improved when T_2 -weighted images are reviewed in parallel with images weighted by water diffusion, dynamic contrast enhancement, and/or ^1H -spectroscopy (1-4,19-20). T_2 quantification may further augment a multi-parametric analysis of prostate cancer, by potentiating auto-segmentation of tumor-dense regions on parametric maps (T_2 , DCE, ADC) and for more comprehensive longitudinal monitoring of tumor response to therapy.

Conclusion

A magnetization-prepared spiral imaging technique was adapted for prostate T_2 quantification with adequate time efficiency, volumetric coverage, and RF insensitivity for clinical piloting. Consistent with prior literature, cohorts without history of external beam irradiation demonstrated significantly prolonged T_2 relaxation in the uninvolved peripheral zone compared to the central gland zone and tumor. Regional T_2 differences were reduced following external beam radiation. SNR must be augmented from that provided by standard phased-array coil acquisitions to guide designs of future trials targeting focal tumor hypoxia and therapy response based on voxel-based T_2 mapping.

Acknowledgements

References:

1. Hricak H, Choyke P, Eberhardt S, Leibel S, Scardino P. Imaging prostate cancer: A multidisciplinary perspective. *Radiology* 2007;243:28-53.
2. Gibbs P, Tozer D, Liney G, Turnbull L. Comparison of quantitative T2 mapping and diffusion-weighted imaging in the normal and pathologic prostate. *Magn Reson Med* 2001;46:1054-1058.
3. Haider M, van der Kwast T, Tanquay J, Evans A, Hashmi A, Lockwood G, Trachtenberg J. Combined T2-weighted and diffusion-weighted MRI for localization of prostate cancer. *Am J Roentgenol* 2007;189:323-328.
4. Langer D, van der Kwast T, Evans A, Sun L, Yaffe M, Trachtenberg J, Haider M. Intermixed normal tissue within prostate cancer: effect on MR imaging measurements of apparent diffusion coefficient and T2-sparse versus dense cancers. *Radiology* 2008;249:900-908.
5. Foltz W, Al-Kwif O, Sussman M, Stainsby J, Wright G. Optimized spiral imaging for measurement of myocardial T2 relaxation. *Magn Reson Med* 2003;49:1089-1097.
6. Foltz W, Stainsby J, Wright G. T2 accuracy on a whole body imager. *Magn Reson Med* 1997;38:759-768.
7. Foltz W, Merchant N, Downar E, Stainsby J, Wright G. Coronary venous oximetry using MRI. *Magn Reson Med* 1999;42:837-848.
8. Brittain J, Hu B, Wright G, Meyer C, Macovski A, Nishimura D. Coronary angiography with magnetization-prepared T2 contrast. *Magn Reson Med* 1995;33:689-696.
9. Cunningham C, Pauly J, Nayak K. Saturated double-angle method for rapid B1+ mapping. *Magn Reson Med* 2006;55:1326-1333.

10. Constantinides C, Atalar E, McVeigh E. Signal-to-noise measurements in magnitude images from NMR phased arrays. *Magn Reson Med* 1997;38:852-857.
11. Kjaer L, Thomsen C, Iversen P, Henriksen O. In vivo estimation of relaxation processes in benign hyperplasia and carcinoma of the prostate gland by magnetic resonance imaging. *Magn Reson Imaging* 1987;5:23-30.
12. Storås T, Gjesdal K, Gadmar O, Geitung J, Kløw N. Prostate magnetic resonance imaging: multiexponential T2 decay in prostate tissue. *J Magn Reson Imaging* 2008;28:1166-1172.
13. Kershaw L, Hutchinson C, Buckley D. Benign prostatic hyperplasia: Evaluation of T1, T2, and microvascular characteristics with T1-weighted dynamic contrast-enhanced MRI. *J Magn Reson Imaging* 2009;29:641-648.
14. Roebuck J, Haker S, Mitsouras D, Rybicki F, Tempny C, Mulkern R. Carr-Purcell-Meiboom-Gill imaging of prostate cancer: quantitative T2 values for cancer discrimination. *Magnetic Resonance Imaging* 2009;27:497-502.
15. Crawley A, Henkelman R. Errors in T2 estimation using multislice multiple-echo imaging. *Magn Reson Med* 1987;4:34-47.
16. Kirkham A, Emberton M, Allen C. How good is MRI at detecting and characterising cancer within the prostate? *Eur Urol* 2006;50:1163-1174.
17. Nakashima J, Tanimoto A, Imai Y, Mukai M, Horiguchi Y, Nakagawa K, Ova M, Ohigashi T, Marumo K, Murai M. Endorectal MRI for prediction of tumor site, tumor size, and local extension of prostate cancer. *Urology* 2004;64:101-105.
18. Haider M, Chung P, Sweet J, Toi A, Jhaveri K, Menard C, Warde P, Trachtenberg J, Lockwood G, Milosevic M. Dynamic contrast-enhanced magnetic resonance imaging for

localization of recurrent prostate cancer after external beam radiation. *Int J Radiat Oncol Biol Phys* 2008;70:425-430.

19. Chen M, Dang H, Wang J, Zhou C, Li S, Wang W, Zhao W, Yang Z, Zhong C, Li G. Prostate cancer detection: comparison of T2-weighted imaging, diffusion-weighted imaging, proton magnetic resonance spectroscopic imaging, and the three techniques combined. *Acta Radiol* 2008;49:602-610.

20. Jackson A, Reinsberg S, Sohaib S, Charles-Edwards E, Jhaver S, Christmas T, Thompson A, Bailey M, Corbishley C, Fisher C, Leach M, Dearnaley D. Dynamic contrast-enhanced MRI for prostate cancer localization. *Br J Radiol* 2009;82:148-156.

Figure Legend:

Figure 1: T2prep design, consisting of sequential intervals for contrast preparation, imaging, and nulling of remnant magnetization. Contrast preparation uses composite 90 and -90 pulses, bracketed around a MLEV train of composite $90x180y90x$ refocusing pulses (4 shown), and a trailing spoiler pulse and gradient. An adiabatic inversion pulse is applied on every even-numbered excitation to preserve T2 contrast during longitudinal storage. Imaging uses a spectral-spatial excitation and spiral imaging gradients, with trailing spoiler gradient. A BIR-4 pulse and trailing spoiler resets the magnetization to ensure constant period of T1 recovery for all echo times.

Figure 2: Quality assurance testing; (a) Coronal B1 map through the phantom. The height of the narrow rectangle demarcates the volume averaged for B1 quantification, while the dashed box demarcates the location of T2 evaluation. The length of the dashed box demarcates the slice package, while the height of the dashed box demarcates the diameter of the ROI for noise-insensitive T2 quantification. (b) T2 variation across sequential imaging slices at RF field offset between approximately -20 and 20%. The T2 error is the percentage standard deviation of T2 measurements across all slices, relative to the T2 value in the central slice at minimal RF offset.

Figure 3: T2prep acquisitions and comparative FSE images acquired from a Cohort A subject throughout the prostate; column (A) Early echo time T2prep image; column (B) late echo time images; and column (C) FSE image. The T2prep images are windowed between 0 and 1200 and 0 and 500 signal units respectively. Similarly, FSE images are windowed between 0 and 500

signal units. Intra-prostatic implanted gold fiducial markers are visible as focal hypo-intensities in some figure panels (white arrows in column (A)).

Figure 4: Representative T2prep acquisitions, acquired at apex, mid (x2), and base locations of the prostate using an endo-rectal coil; Column (A) Early echo time images, windowed between signal intensities of 0 and 1000 (256 grey levels); Column (B) late echo time images, windowed between signal intensities of 0 and 500 (256 grey levels); and (c) T2 maps, windowed between T2 values of 0 and 200ms (256 grey levels). Three intra-prostatic implanted gold fiducial markers are visible as focal hypo-intensities in Column (A), and demarcated with the black arrows.

Figure 5: Representative images for Cohort A (top rows) and Cohort B (bottom rows), displaying tumors as nodular hypointensities in diagnostic fast-spin-echo, T2-weighted T2prep images, and T2 maps created from T2prep images at echo times of 3 and 88ms. The T2 maps are windowed between 0 and 200ms.

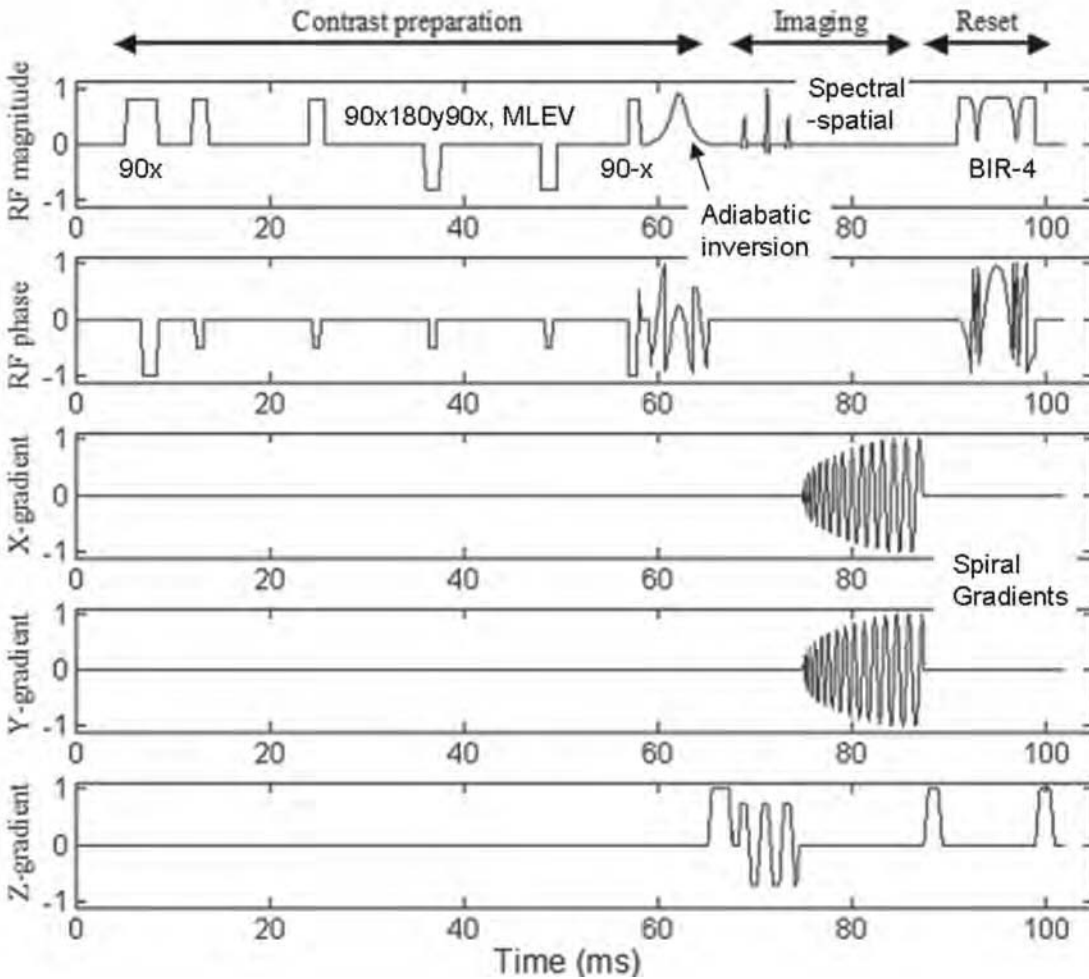


Figure 1: T2prep design, consisting of sequential intervals for contrast preparation, imaging, and nulling of remnant magnetization. Contrast preparation uses composite 90 and -90 pulses, bracketed around a MLEV train of composite $90x180y90x$ refocusing pulses (4 shown), and a trailing spoiler pulse and gradient. An adiabatic inversion pulse is applied on every even-numbered excitation to preserve T2 contrast during longitudinal storage. Imaging uses a spectral-spatial excitation and spiral imaging gradients, with trailing spoiler gradient. A BIR-4 pulse and trailing spoiler resets the magnetization to ensure constant period of T1 recovery for all echo times.

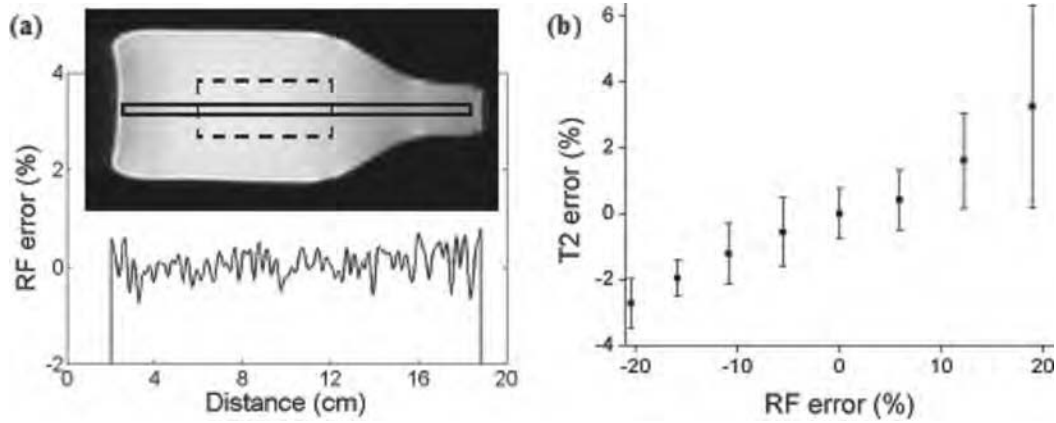


Figure 2: Quality assurance testing; (a) Coronal B1 map through the phantom. The height of the narrow rectangle demarcates the volume averaged for B1 quantification, while the dashed box demarcates the location of T2 evaluation. The length of the dashed box demarcates the slice package, while the height of the dashed box demarcates the diameter of the ROI for noise-insensitive T2 quantification. (b) T2 variation across sequential imaging slices at RF field offset between approximately -20 and 20%. The T2 error is the percentage standard deviation of T2 measurements across all slices, relative to the T2 value in the central slice at minimal RF offset.

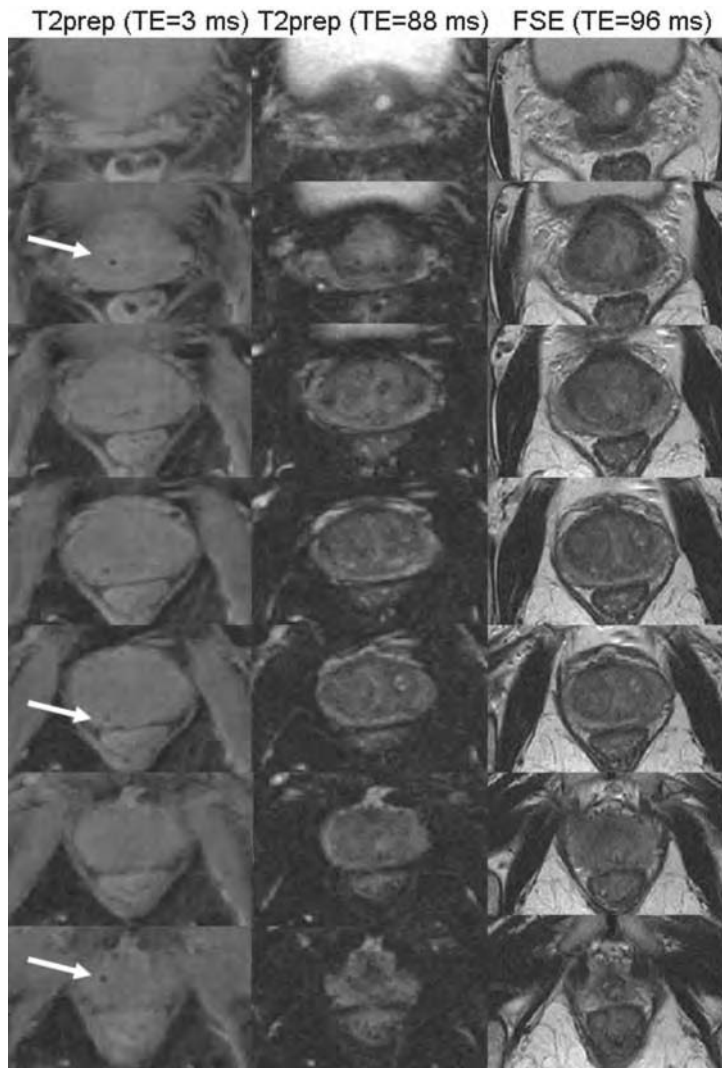


Figure 3: T2prep acquisitions and comparative FSE images acquired from a Cohort A subject throughout the prostate; column (A) Early echo time T2prep image; column (B) late echo time images; and column (C) FSE image. The T2prep images are windowed between 0 and 1200 and 0 and 500 signal units respectively. Similarly, FSE images are windowed between 0 and 500 signal units. Intra-prostatic implanted gold fiducial markers are visible as focal hypo-intensities in some figure panels (white arrows in column (A)).

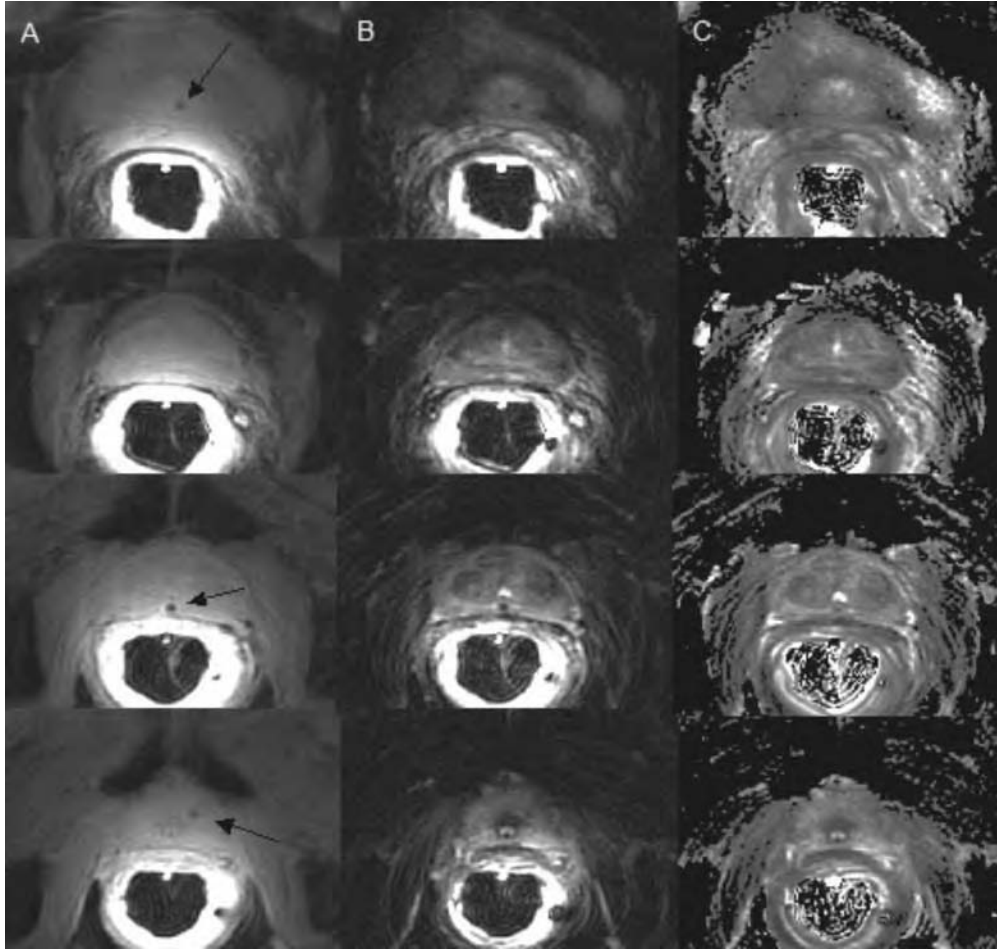


Figure 4: Representative T2prep acquisitions, acquired at apex, mid (x2), and base locations of the prostate using an endo-rectal coil; Column (A) Early echo time images, windowed between signal intensities of 0 and 1000 (256 grey levels); Column (B) late echo time images, windowed between signal intensities of 0 and 500 (256 grey levels); and (c) T2 maps, windowed between T2 values of 0 and 200ms (256 grey levels). Three intra-prostatic implanted gold fiducial markers are visible as focal hypo-intensities in Column (A), and demarcated with the black arrows.

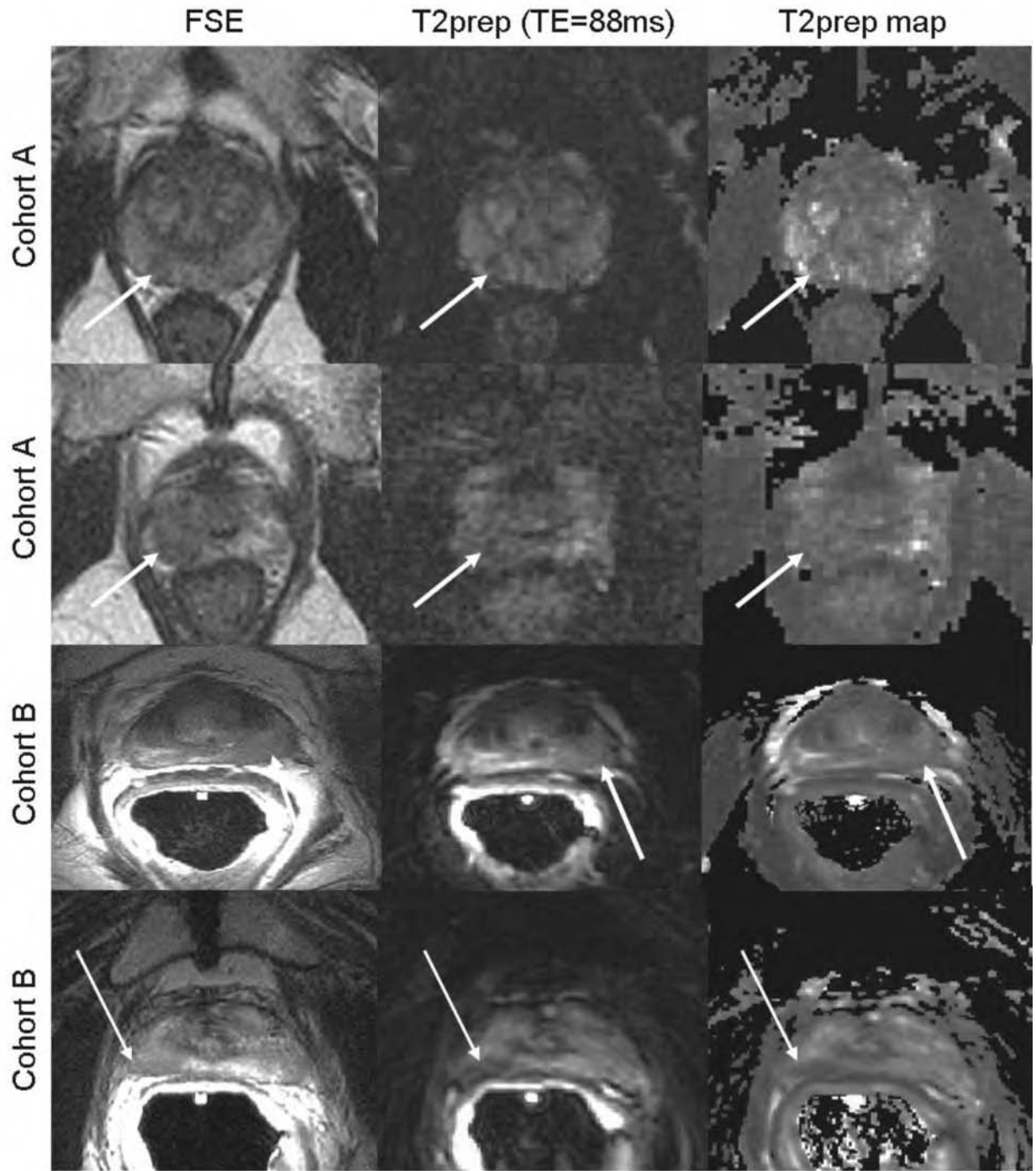


Figure 5: Representative images for Cohort A (top rows) and Cohort B (bottom rows), displaying tumors as nodular hypointensities in diagnostic fast-spin-echo, T2-weighted T2prep images, and T2 maps created from T2prep images at echo times of 3 and 88ms. The T2 maps are windowed between 0 and 200ms.